*TNO report*
PML 1997-A65

# Behind-armour Debris Modelling for High-velocity Fragment Impact (Part 2)


TNO Prins Maurits Laboratory

Lange Kleiweg 137
P.O. Box 45
2280 AA Rijswijk
The Netherlands

Phone +31 15 284 28 42
Fax +31 15 284 39 59


Date
December 1997


Author(s)
Dr. J.L. Verolme




| | | |
|---|---|---|
| Classification | | |
| Classified by | : | Major J.H.J. Verhulst |
| Classification date | : | 18 November 1997 (this classification will not change) |
| Title | : | Ongerubriceerd |
| Managementuittreksel | : | Ongerubriceerd |
| Abstract | : | Ongerubriceerd |
| Report text | : | Ongerubriceerd |
| Annexes A - B | : | Ongerubriceerd |



| | | |
|---|---|---|
| Copy no. | : | 13 |
| No. of copies | : | 31 |
| No. of pages | : | 42 (incl. annexes, excl. RDP & distribution list) |
| No. of annexes | : | 2 |

All information which is classified according to Dutch regulations shall be treated by the recipient in the same way as classified information of corresponding value in his own country. No part of this information will be disclosed to any party.

The classification designation Ongerubriceerd is equivalent to Unclassified.



TNO Prins Maurits Laboratory is part of
TNO Defence Research which further consists of:

TNO Physics and Electronics Laboratory
TNO Human Factors Research Institute

Netherlands Organization for
Applied Scientific Research (TNO)

# Managementuittreksel

| | | |
|---|---|---|
| Titel | : | Behind-armour Debris Modelling for High-velocity Fragment Impact (Part 2) |
| Auteur(s) | : | Dr. ir. J.L. Verolme |
| Datum | : | december 1997 |
| Opdrachtnr. | : | A94KLu423 |
| Rapportnr. | : | PML 1997-A65 |

Ter verkrijging van kennis inzake de mechanismen van schadevorming aan materialen ten gevolge van inslag van snelle fragmenten, heeft DMKLu het TNO Prins Maurits Laboratorium (TNO-PML) verzocht een onderzoeksproject uit te voeren; deze opdracht heeft het nummer A94KLu423 en draagt als titel 'Inslag van hogesnelheidsfragmenten op luchtdoelen'. Dit onderzoek strekt zich uit over zes jaar. De resultaten van de eerste fase van dit onderzoek, een literatuurstudie en een serie verkennende experimenten, zijn beschreven in een TNO-rapport.[1] Fase 2 omvat het uitvoeren van experimenten op enkelvoudige en meervoudige doelen. Een eerste rapport over deze fase is reeds verschenen.[2] In dit rapport wordt dit deelonderzoek verder beschreven.
Inslagexperimenten zijn uitgevoerd met korte cylinders van wolfraam en staal. Deze zijn afgevuurd op ten eerste enkelvoudige platen van pantserstaal onder diverse invalshoeken. Ten tweede is een aantal experimenten uitgevoerd op een meervoudig platendoel, dat een gevechtshelikopter modelleert. Voor het karakteriseren van de fragmentenbundel achter de doelplaat is gebruikgemaakt van getuigenpakketten, arrays van in dit geval stalen platen met daartussen polystyreen. Uit deze getuigenpakketten kon het aantal fragmenten en de verdeling gehaald worden. Tevens is, bij sommige experimenten, de fragmentenwolk op twee tijdstippen gefotografeerd om het snelheidsverloop te bepalen.
Uit de experimenten bleek dat bij inslagsnelheden boven ongeveer 1200 m/s het wolfraam projectiel volledig opbrak door de interactie met de RHA-doelplaat. Uit deze experimenten is een aantal tendenzen gehaald. Door het geringe aantal experimenten moeten alle conclusies met enige terughoudendheid worden beschouwd. Naarmate de inslagsnelheid toeneemt:

- neemt het aantal fragmenten toe;
- neemt de grootte van de fragmenten af;
- neemt de maximale doordringdiepte in het getuigenpakket af (dus de energie van ieder deeltje afzonderlijk);

---

1 Ingen, R.P. van,
'Inslag van hoge-snelheidsfragmenten op luchtdoelen: een verkennende studie',
TNO-rapport PML 1996-A14, juni 1996.

2 Verolme, J.L.,
'Inslag van hoge-snelheidsfragmenten op luchtdoelen. 'Behind Armour Debris' modellering en oriënterende experimenten',
TNO-rapport PML 1997-A4, april 1997.

- wordt de bundel waarin fragmenten worden aangetroffen breder;
- neemt de grootte van het gat in de doelplaat toe.

Naarmate de inslaghoek toeneemt (ten opzichte van de normaal van de doelplaat), neemt het aantal gaten in de eerste plaat van het getuigenpakket af, zowel voor wolfraam als voor staal.
Het stalen projectiel brak, in tegenstelling tot het wolfraam, niet op, maar 'erodeerde' weg. Dit is duidelijk aan de schade in de getuigenpakketten te zien, zowel aan het aantal gaten als aan de indringdiepte.
Simultaan met de experimenten is een model ontwikkeld dat met behulp van een combinatie van hydrocodeberekeningen en een aantal semi-empirische relaties de hoofdkarakteristieken van de fragmentenbundel kan voorspellen. Met deze karakteristieken wordt de schade aan het getuigenpakket voorspeld. Deze schade kan dan worden vergeleken met die in de praktijk.
Voor het verbeteren van het model is een studiereis naar de USA gemaakt door de auteur/projectleider. In het hoofdstuk over modelleren worden de resultaten van het overleg met een aantal experts op het gebied van modelleren van fragmentatie gepresenteerd.
Het model kan de fragmentenverdeling en de snelheidsverdeling van de voorkant van de wolk als functie van de emissiehoek goed voorspellen. Verdere aandacht moet worden gericht op het voorspellen van het aantal gaten in de eerste plaat van het pakket. De resultaten zijn bevredigend, maar kunnen nog aanzienlijk worden verbeterd door gericht vervolgonderzoek.
In de volgende fase zullen verdere experimenten worden uitgevoerd met andere doelmaterialen, om het model te verbeteren en het toepassingsgebied te vergroten. Ook zal het model worden uitgebreid om het in de praktijk vaak voorkomende niet-loodrechte inslaan van projectielen op doelplaten te beschrijven.

# Contents

# 1 Introduction

In flying weapon platforms modern structural materials like composites, titanium and fiber metal laminates are increasingly used. Little is known about the ballistic performance of such materials, especially in the high-velocity regime. High effective impact velocities, even up to 2.5 km/s, can result from the head-on interaction of particles originating from fragmenting warheads with flying air targets. An additional complicating factor is the ever-increasing use of high-density fragment material, such as tungsten. Due to the high engagement speeds, these fragments may break-up, causing a highly lethal, highly dispersed cloud of small, high-energy debris.

A research project was defined studying the above mentioned high-velocity impact of modern, high-density fragments on modern air-target materials. This project consists of three phases. The results of the first phase, a survey of literature and some exploratory experiments, are described in [1]. Performing experiments with tungsten and steel fragments on single and multiple plate targets is the second and third phase. In the second, attention is focussed on classical materials, while in phase three modern target materials will be evaluated. Parallel, a model is being developed to predict the fragmentation properties of materials. The results of phase 2 are presented in [2] and this report.

In Chapter 2 the experiments are described. The test set-up is explained and the most important results are presented. Chapter 3 contains a description of the fragmentation model. In Chapter 4 the hydrocode simulations are presented. Chapter 5 gives an overview of the correlation of the model and the experimental results is given. An evaluation can be found in Chapter 6.

# 2 Experiments

For the quantification of fragmentation properties steel and tungsten projectiles were fired at rolled homogeneous armour (RHA) plates (type ARMOX 370W, with a Brinell hardness $HB_{30}$ of 370). The projectiles were cylinders with a length to diameter ratio of 1. The mass was 35 (tungsten) and 16 (steel) gram. The cylinders had a diameter of 13 mm. The impact velocities were varied between 1 km/s and 2.5 km/s.
In addition, the same projectiles were fired at an array of plates, representing an armoured helicopter. The first plate of this multiple-plate array is a 10.4 mm RHA plate. The next section gives the results for the single plate and multiple plate targets respectively.

## 2.1 Single-plate targets

The full test matrix for the experiments with the single-plate targets is given in Table 1. In two additional tests (not in the table), at 902 and 1178 m/s, the tungsten projectile did not break up. The test setup is equal to the earlier experiments [2]. For the acceleration of the projectile and sabot, a 78 mm smoothbore laboratory powder gun was used. The projectile velocity was measured by means of both break-screens and inductive coils. Two orthogonal flash X-ray units were used to measure in two planes (yaw and pitch) prior to impact. The lateral target plate dimensions were 40 by 40 cm. At a distance of 50 cm behind the target-plate, the witness pack was placed. The witness pack was 1 by 1 meter for the normal impact, and 2 by 1 meter for the off-normal impact experiments (obviously to catch all debris particles). The witness pack consisted of 6 mild steel (St.37-2 or St.12-3) plates, placed at a distance of 25.4 mm with polystyrene in between. To secure the distance of 25.4 mm, the plates were bolted at 8 positions with spacers inbetween the plates. The thicknesses of the witness pack plates were respectively 0.8, 1.5, 1.5, 3.0, 3.0 and 6.0 millimeter, measured in the direction of the line of fire [2]. For oblique impact the setup of the witness pack is shown in Figure 1.

*Table 1: Test matrix.*

| I.D. | Projectile | Target | Angle of Obliquity (°NATO) | Velocity (m/s) |
|---|---|---|---|---|
| 3552 | Tungsten | 10 mm RHA[1] | 0 | 1885 |
| 3553 | Tungsten | " | 0 | 1514 |
| 3555 | Tungsten | " | 0 | 1779 |
| 3556 | Tungsten | " | 0 | 1449 |
| 3855 | Steel | " | 0 | 1477 |
| 3856 | Tungsten | 20 mm RHA | 0 | 1525 |
| 3857 | Tungsten | 10 mm RHA[1] | 0 | 2444 |
| 3858 | Steel | " | 0 | 2419 |
| 3859 | Steel | " | 30 | 1567 |
| 3860 | Tungsten | " | 30 | 2438 |
| 3861 | Steel | " | 30 | 2396 |
| 3862 | Tungsten | " | 60 | 2416 |
| 3863 | Steel | " | 60 | 2400 |

*1* Actual thickness 10.4 mm.

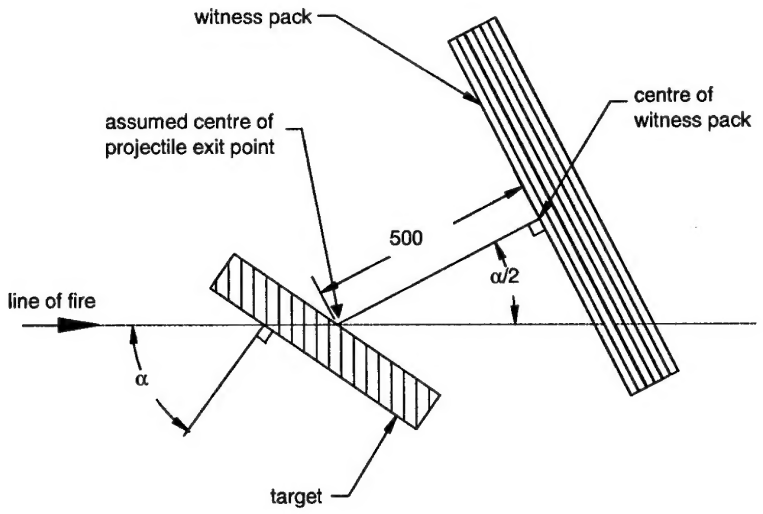


*Figure 1: Target and witness pack setup.*

Experiments 3552 to 3556 were already reported in [2], but will be included in this report as well, for the sake of completeness. Only for these four experiments X-ray pictures were used to obtain a velocity distribution in the debris cloud.
Table 2 presents the most important test results for the normal impact experiments: the inner diameter of the hole in the target plate, the number of holes in the first witness pack plate, the maximum emission angle, and the total yaw. The emission angle is defined as the angle between the normal to the centre of the witness pack and the trajectory of the debris fragment. This data is presented in emission angle segments of 5°, therefore the value in Table 2 is always a multiple of 5. The total yaw $\varphi$ is defined as:

$$\varphi = \sqrt{\varphi_{xx}^2 + \varphi_{yy}^2} \quad (1)$$

where the subscripts xx and yy indicate the two measured components, the yaw and the pitch.

It can be concluded from the table that the behind-armour effects of tungsten are more severe than steel. At nearly the same velocity much less holes in the witness pack are observed for steel than for tungsten. The maximum emission angle is seen to increase as a function of the impact velocity. The total yaw of the projectile prior to impact was considerable. Attention should be focussed on the influence of yaw on the test results.

*Table 2: Test results for normal-impact experiments.*

| I.D. | Code[1] | D (mm)[2] | $H_1$[3] | $\theta_{max}$ (°)[4] | M (gr)[5] | $\varphi$ (°)[6] |
|---|---|---|---|---|---|---|
| 3556 | T10/1449 | 20 | 270 | 30 | 32 | - |
| 3553 | T10/1514 | 22 | 336 | 35 | 31 | - |
| 3555 | T10/1779 | 23 | 529 | 40 | 42 | - |
| 3552 | T10/1885 | 30 | 600 | 35 | 50 | - |
| 3857 | T10/2444 | 30 | 802 | 50 | 63 | 8.1 |
| 3856 | T20/1525 | 24 | 83 | 40 | 92 | 10.8 |
| 3855 | S10/1477 | 22 | 38 | 35 | n/a | 11.2 |
| 3858 | S10/2419 | 31 | 357 | 50 | 54 | 27.2 |

*1* Experiment code: projectile material T = tungsten, S = steel, target thickness in millimeter, and velocity in m/s.

*2* Target hole diameter.

*3* Number of holes in first witness pack plate.

*4* Maximum emission angle (assuming rotational symmetry).

*5* Mass loss of target plate.

*6* Total yaw.

For normal impact of tungsten at 10 mm of RHA, Figure 2 shows a general trend: the penetrative capability of the fragments decreases as the impact velocity increases. In addition, the number of fragments is increasing with increasing velocity.

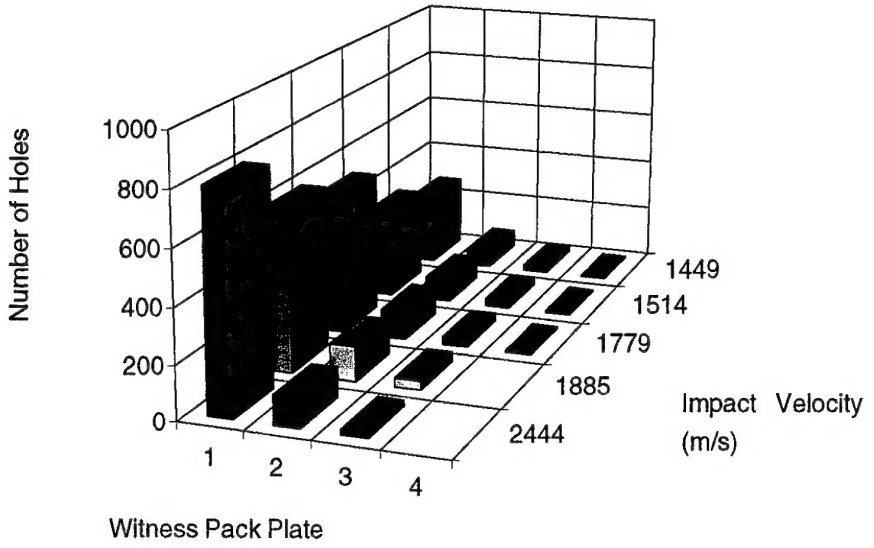


*Figure 2: The number of holes in the witness pack for normal impact of tungsten cylinder on 10 mm of RHA.*

Figure 3 presents for normal impact the inner diameter of the hole in the target plate as a function of the impact velocity. One general liner trend appears to dominate the behaviour for steel and tungsten, independent also of the target plate thickness.

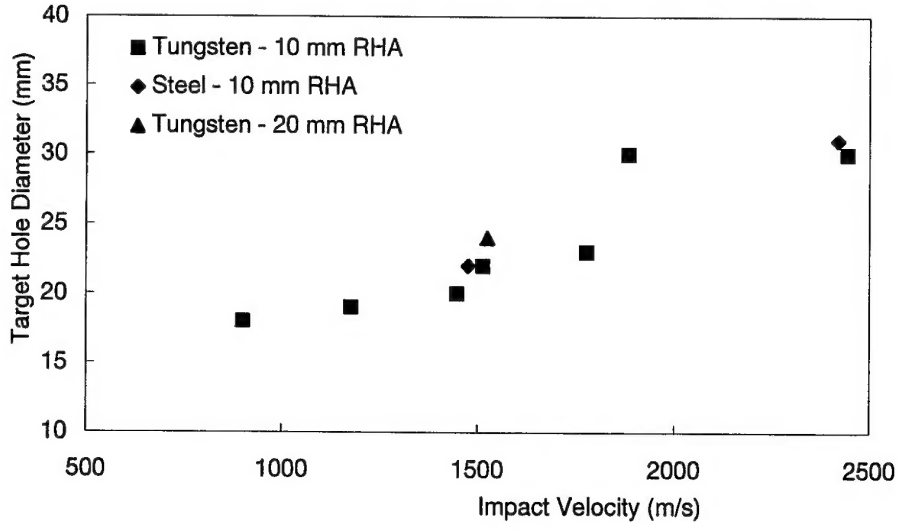


*Figure 3: Target hole diameter as a function of the impact velocity.*

It was already shown in [2] that the correlation between the target inner-hole diameter and the equivalent diameter determined by the experimental mass loss of the target plate is good (assuming that the density of the target-plate material is 7.83 g/cm$^3$). Table 3 illustrates that using the mass loss only leads to predictions within 10% for all normal impact experiments.

*Table 3: Hole diameters for normal impact.*

| I.D. | Code | D (mm) | M (g) | $D_{eq}$ (mm)[1] | $D/D_{eq}$ |
|---|---|---|---|---|---|
| 3556 | T10/1449 | 20 | 32 | 22 | 0.91 |
| 3553 | T10/1514 | 22 | 31 | 22 | 1.00 |
| 3555 | T10/1779 | 23 | 42 | 26 | 0.88 |
| 3552 | T10/1885 | 30 | 50 | 28 | 1.07 |
| 3857 | T10/2444 | 30 | 63 | 30 | 1.00 |
| 3856 | T20/1525 | 24 | 92 | 27 | 0.89 |
| 3855 | S10/1477 | 22 | n/a | n/a | n/a |
| 3858 | S10/2419 | 31 | 54 | 30 | 1.03 |

*1* Equivalent diameter.

For the off-normal impact experiments, the most important results are presented in Table 4.

*Table 4: Test results for oblique impact experiments.*

| I.D. | Code[1] | D (mm)[2] | $H_1$[3] | $\theta_{max}$ (°)[4] | φ (°)[5] | M (gr)[6] |
|---|---|---|---|---|---|---|
| 3860 | 30T10/2438 | 28/34 | 690 | 45/50/40 | - | 71 |
| 3862 | 60T10/2416 | 29/47 | 321 | 50/45/40 | 10.6 | 95 |
| 3859 | 30S10/1567 | 24/28 | 13 | 25/15/15 | - | 41 |
| 3861 | 30S10/2396 | 27/30 | 211 | 50/35/40 | 17.5 | 64 |
| 3863 | 60S10/2400 | 22/35 | 3 | 20/20/20 | 37.0 | 49 |

*1* Experiment code: angle of obliquity, projectile material T = tungsten, S = steel, target thickness in millimeter, and velocity in m/s.

*2* Target hole sizes (the two chords of an ellipse).

*3* Number of holes in first witness pack plate.

*4* Maximum emission angles in 0, 90 and 180° direction (elliptical distribution, assuming one line of symmetry).

*5* Total yaw.

*6* Mass loss.

In Figure 4 the number of holes in the first plate of the witness pack is given as a function of both the impact velocity and the angle of obliquity for a 10 mm RHA target.

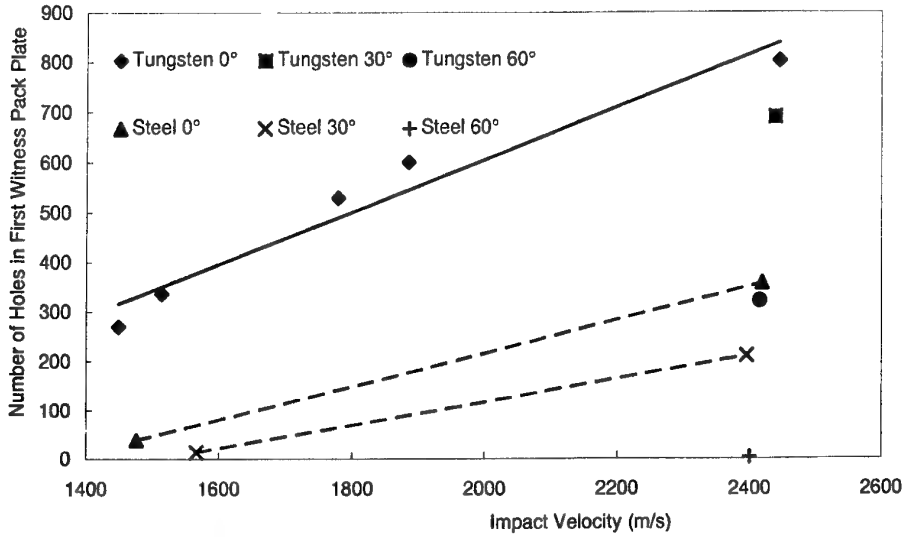


*Figure 4: Number of holes in first witness pack plate as function of impact velocity and angle of obliquity.*

For an increasing obliquity, the number of holes is seen to decrease. In the figure a linear dependency is assumed, merely only to show the general behaviour.
The experimental data collected from the witness pack is given in Annex A. There per experiment two tables are given. The first gives the number of perforations per emission angle segment. Recall that the emission angle is the angle between the normal to the centre of the witness pack and the fragment trajectory angle. In the second table for area classes the number of perforations are tabled. In these tables for normal impact it is assumed that the debris cloud is axisymmetric with respect to the centre of the witness pack, which is in this case coinciding with the line of fire. In all cases this assumption seemed to be justified.
Some general conclusions on the witness pack hole distribution are:

- the highest number of perforations is observed in the emission angle segment between 5 and 15 degrees. This indicates that a normal distribution should model the behaviour best;
- most holes (60 to 80%) are small, in the area class of 0-10 $mm^2$.

For oblique impact it was assumed that the debris cloud was line symmetrical (see Figure 1; symmetry plane is the plane of the paper).
Most fragments are found in the sector 135-180°. For the 30° obliquity most perforations are within the emission angle segment of 15 - 25°, while for 60° obliquity this range is 20 to 30°. These effects are explained in Figure 5. Here the results shown above are visualized for experiment 3862.
In case of oblique impact the behind-armour debris is always directed towards the normal to the target plate. The deviation angle of the centre of mass of the debris can be roughly approximated by half the angle of obliquity of the target plate. This explains the emission angle segments where most perforations are found. The residual penetrator and/or the fragments originating from the penetrator behind the

target are always found near the line of fire. This explains the sector 135-180° where most fragments are found (see Figure 5 for the definition of the sector angles).

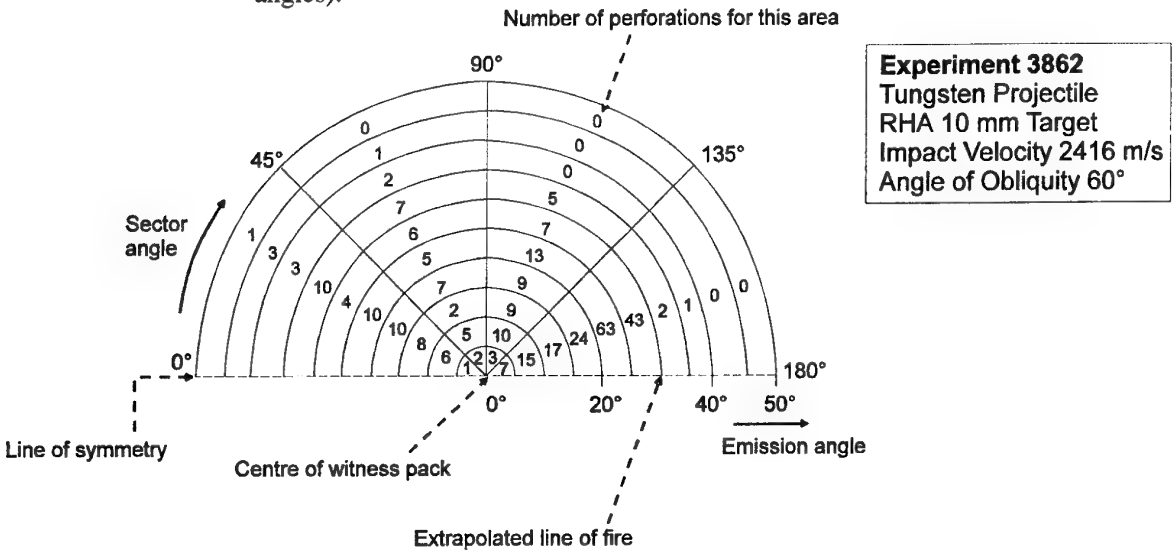


*Figure 5: Graphical representation for the results of oblique experiment 3862.*

Basically the same trends can be observed. The only differences are the smaller amount of holes found and the lower penetrative capacity of the fragments for steel, as compared to tungsten.

## 2.2 Multiple-plate targets

For the multiple plate targets, Table 5 gives the testmatrix.

*Table 5: Test matrix for multiple-plate experiments.*

| I.D. | Projectile | Target | Velocity (m/s) |
|---|---|---|---|
| 3864 | Steel | Helicopter | 2420 |
| 3865 | Tungsten | " | 1750 |
| 3866 | Tungsten | " | 2486 |
| 3867 | Tungsten | " | 2084 |

The helicopter target is depicted in Figure 6. The materials used are mild steel (St.37), RHA (ARMOX 370W) and aluminium (Dural ALCuMg 1 F40).

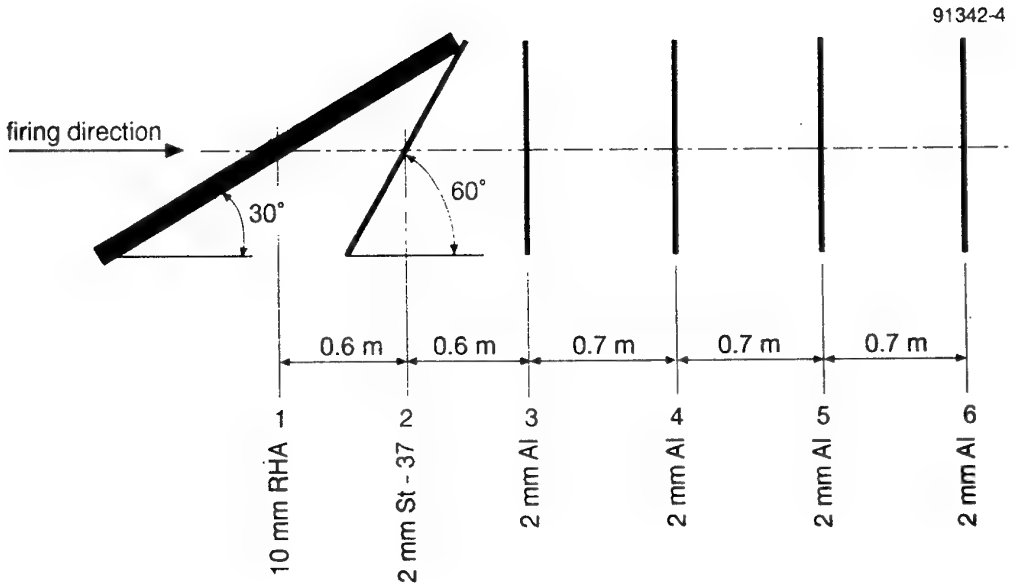


*Figure 6: Helicopter simulation target.*

Figure 7 shows the number of holes per plate for the four different shots. It is obvious that tungsten, being the more brittle material, causes much more damage (much more holes, penetrating deeper into the target) as compared to steel. A steel fragment at 2400 m/s causes only a limited number of holes (6) in the second steel plate, while a tungsten fragment at approximately the same velocity causes 110 holes in the second steel plate, and even 12 holes in the last (6th) plate.

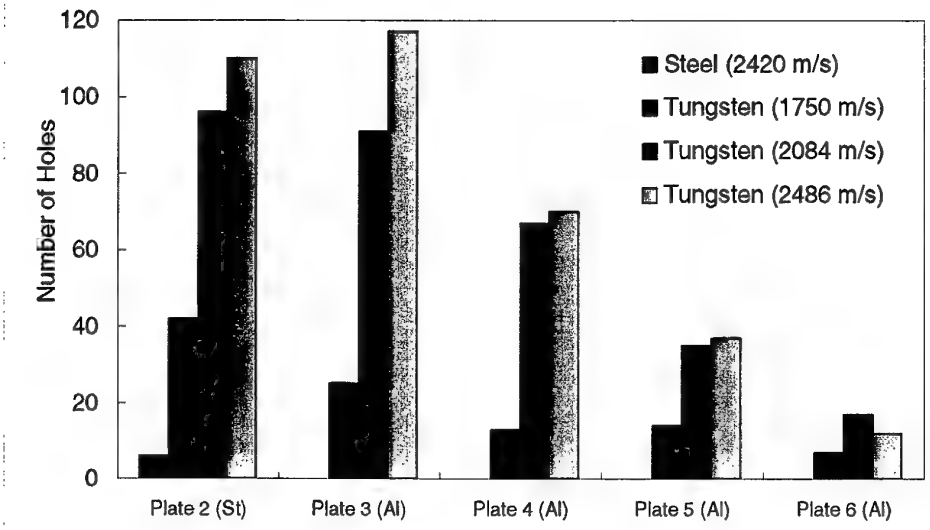


*Figure 7: Number of holes per plate for the helicopter target.*

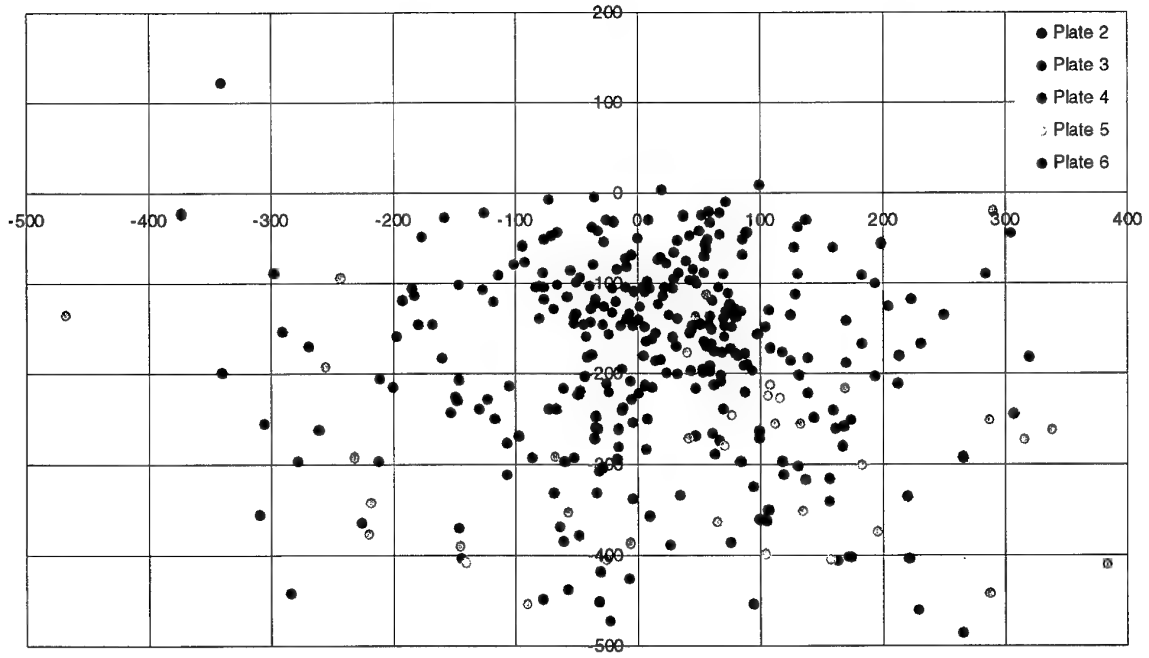


*Figure 8: Damage pattern to helicopter target for shot 3866 (tungsten, 2486 m/s).*

Figure 8 shows the distribution of the holes in the plates of the multiple plate target. In this figure, the origin is the line of fire. Basically the same elliptical distribution can be observed than in the oblique experiments. Because of the interaction with the first plate (under 60° NATO), most of the behind-armour debris originating from this steel plate is shifted towards the negative Y-axis of

Figure 8. As a consequence, unfortunately several fragmens were 'lost' because of the limited size of the plates in negative Y-direction.

Table 6 gives an overview of the most important results, a full overview of the data is given in Annex B.

*Table 6: Test results for multiple-plate experiments.*

| I.D. | Code[1] | D (mm)[2] | φ (°)[3] | M (g)[4] |
|---|---|---|---|---|
| 3864 | S/2420 | 22/26 | 10 | 44 |
| 3865 | T/1750 | 23/38 | 10 | 65 |
| 3867 | T/2084 | 26/38 | 4.2 | 72 |
| 3866 | T/2486 | 30/45 | 11.1 | 89 |

*1* Experiment code: projectile material T = tungsten, S = steel, and velocity in m/s.

*2* Elliptical target hole dimensions.

*3* Total yaw.

*4* Mass loss.

The four tables of Annex B give the hole pattern for the plates in the same format as the data presented before for the oblique impact. However, here the origin is the extrapolated line of fire.
For the steel fragment at 2420 m/s hardly any damage is observed. The fragment is only capable of penetrating one plate behind the RHA plate. The effect of using tungsten as fragment material is much more severe.

# 3 Modeling

Air target vulnerability estimates require penetration models for fragment-target interactions at impact velocities up to 3 km/s. At low speeds, fragments perforate targets without mass loss and do not desintegrate. The ballistic threat in this region can be reasonably represented by a single fragment. As speed rises, some mass may be sheared off as it perforates. When speeds increase even more, fragments can start to break up upon impact, creating a highly lethal, highly dispersed cloud of high-energy fragments. In this region, each fragment can cause a lot of damage and must thus be taken into account. This chapter presents a model which can characterise a debris cloud generated by the impact of a brittle impactor of frangible material at velocities considerably higher than the velocity at which complete break-up takes place, defined here as the shatter velocity.
A schematic of the normal-impact phenomenon is given in Figure 9.

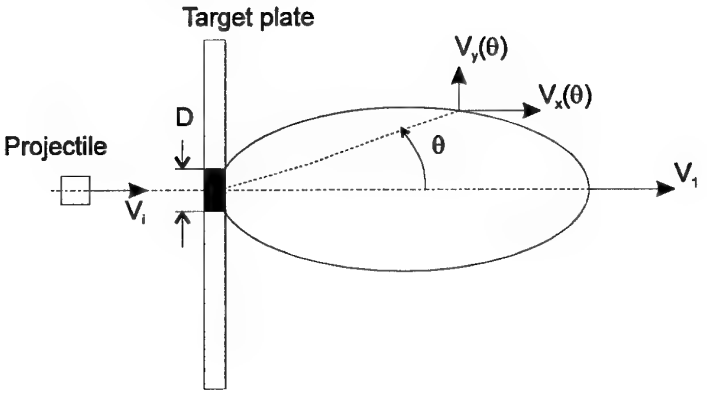


*Figure 9: Schematic representation of high-speed normal-impact process.*

In the model a number of basic assumptions is used.

- All debris cloud particles are located on the periphery of the expanding elliptical shell shown in Figure 9. This assumption is used in most models predicting debris clouds.[3]
- Impact takes place without yaw. In general for a chunky projectile (L/D approximately one) this is a very good assumption.[4]
- Every debris particle is assumed spherical in shape.

---

3 Personal communication with Jerry Yatteau, Applied Research Associates (Denver, Colorado, USA). He is one of the developers of FATEPEN, the Fast Air Target Encounter Penetration tool.

4 Personal communication with Dennis Grady and Marlin Kipp of Sandia National Labs (Albuquerque, New Mexico, USA).

**Shatter velocity**[5]

For the model it is essential to have an estimate of the velocity at which the fragment breaks-up fully (the shatter velocity) for the combination of penetrator and target material. Here an exact value of the impact velocity is not very necessary since in general the highest encounter speed (head-to-head collision: the vector sum of the speed of the air target and the speed of the fragment) is known and cannot be varied. Thus at that velocity a fragment will either shatter or not. In order to roughly predict the shatter velocity one can use earlier obtained experimental values for known material combinations.

When a curve is generated of the normalized largest fragment mass versus the impact velocity a figure similar to Figure 10 is obtained.

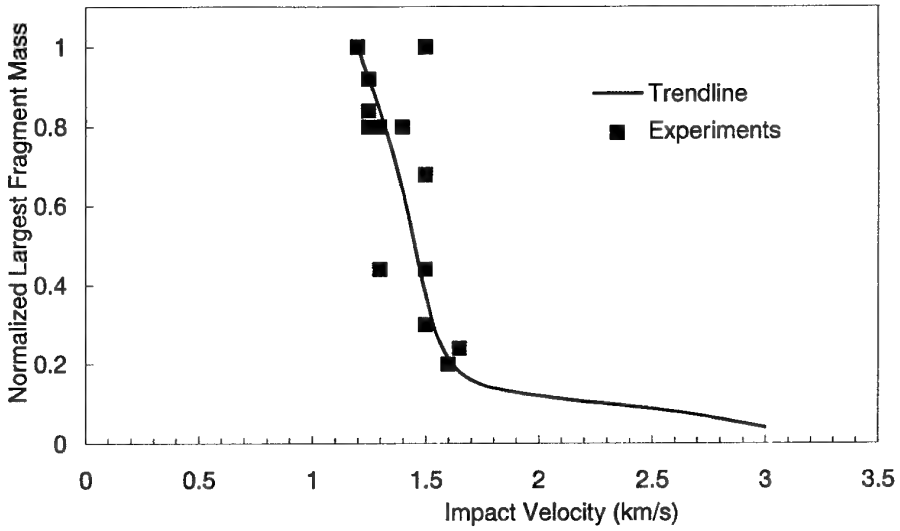


*Figure 10: Normalized largest fragment mass versus impact velocity (fictive data).*

The transition from an intact to a fully-shattered penetrator is seen to occur within a very narrow impact velocity band. It is therefore justified to determine one single shatter velocity without the specification of a bandwidth.

For a very rough first estimate it can be assumed that only the impedance mismatch determines shattering. Normally also a material characteristic like the fracture toughness and the ratio of impactor diameter to target thickness should be taken into account. Notice that for example as a function of the amount of alloying elements and/or heat treatments the impedance hardly changes, but the fracture toughness does. This effect is however not modeled here.

5 Personal communication with Charly Anderson of the Southwest Research Institute (San Antonio, Texas, USA). Nonpublished presentation of C. Anderson.

Define a nondimensional shatter coefficient S as:

$$S = \frac{V_s(\rho_p C_p + \rho_T C_T)}{\rho_p C_p^2} \qquad (2)$$

| | | |
|---|---|---|
| where | $V_s$ | shatter velocity (m/s) |
| | $\rho$ | density (kg/m$^3$) |
| | C | stress wave velocity (m/s) |
| and the indices | T | target |
| | p | projectile |

Table 8 gives known experimental shatter velocities for some material combinations [4]. Using these values leads to a shatter coefficient which is also given in Table 8. The material properties used are listed in Table 7. Although the shatter velocities are for cubes, some experimental evidence has shown that cylinders behave similar.

*Table 7: Material properties for several materials.*

| | $C_0$ (km/s)[1] | $\rho$ (gr/cm$^3$) |
|---|---|---|
| Steel 4140 | 4.61 | 7.83 |
| Graphite Epoxy | 5.81 | 1.58 |
| Steel 1018 | 4.61 | 7.83 |
| Brass | 3.74 | 8.60 |
| Aluminum 2024-T3 | 5.38 | 2.71 |

*1* Stress wave speed determined by bulk modulus.

*Table 8: Shatter velocities for several impact conditions.*

| | Shatter velocity (km/s) | Shatter coefficient S |
|---|---|---|
| Steel 4140 - 2024-T3 | 1.19 | 0.36 |
| Steel 4140 - Graphite epoxy | 1.70 | 0.46 |
| Steel 4140 - Steel 1018 | 0.85 | 0.37 |
| Steel 4140 - Brass | 0.80 | 0.33 |

It appears correct as a first estimate to use a shatter coefficient S of 0.36 for metal to metal impact. The only exception is the steel to graphite-epoxy impact. It is anticipated that this is caused by the non-metallic graphite epoxy.
Due to the small amount of validation data this method to predict the shatter velocity should be used with great caution, and as a means to have a very rough first estimate only.

**Fragmented mass**

When the target plate hole diameter is known and the impact velocity lies well above the shatter velocity, one can determine the total fragmented mass.

The following relation determines the equivalent hole diameter D (determined as the best fit to the experimental data obtained here) [2]:

$$D/d_p = 3.4\left(\frac{t_T}{d_p}\right)^{2/3}\left(\frac{V_i}{C_T}\right) + 0.8 \qquad (3)$$

where
- D target hole diameter (mm)
- $d_p$ diameter of projectile (mm)
- $t_T$ thickness of the target (mm)
- $V_i$ impact velocity (m/s)
- $C_T$ stress wave speed in target (m/s)

The total fragmented mass is equal to the sum of the mass of the projectile $M_p$ and the mass behind the armour plate originating from the target $M_T$. The latter contribution can be estimated with the following equation:

$$M_T = 0.9\frac{\pi}{4} D^2\, t_T\, \rho_T \qquad (4)$$

This equation accounts for both the mass ejected towards the entrance side (about 20%) and the ring-shaped spall or lip fragments at the exit side which causes a deviation from the assumed pure cylindrical hole shape.

**Mass distribution**

An efficient estimate for the average fragment size can be obtained with Grady and Kipp's energy formalism [2]. For the determination of the average fragment size an indication of the strain rate at failure is necessary. Up to approximately 3 km/s fragmentation is determined by the dynamic fracture toughness of the material. In this region no yield-strength dominated fragmentation takes place nor liquid particles are formed. For strain rates from $10^3$ to $10^6$, the following formula gives an indication of the average fragment size d [2]:

$$d = \left(\frac{\sqrt{24}\, K_{Ic}}{\rho\, C \dot{\varepsilon}}\right)^{2/3} \qquad (5)$$

where
- $K_{Ic}$ dynamic fracture toughness $(MPa(m)^{0.5})$
- $\dot{\varepsilon}$ strain rate (1/s)

The strain rate can be approximated by the ratio of the lateral expansion velocity of the cloud and the diameter of the projectile [4]. The lateral expansion velocity can for instance be obtained with hydrocode simulations (see next chapter). With equation (5) and assuming that each particle is a perfect sphere the average fragment mass $m_a$ can be easily obtained:

$$m_a = \frac{\pi}{6}\rho\, d^3 \qquad (6)$$

Knowing the average mass and the total fragmented mass, the number of particles is easily obtained.

With the average fragment size the mass distribution in the debris cloud can be obtained. Here we assume a bilinear distribution [3] of the following form. The number of particles larger than a certain mass m in a distribution $N_i(m)$ is:

$$N_i(m) = \left(\frac{N_i}{6}\right) e^{-\frac{m}{3\,m_{a,i}}} + \left(\frac{5N_i}{6}\right) e^{-\frac{m}{0.6\,m_{a,i}}} \tag{7}$$

Here N is the total number of particles for either the projectile (index i = p) or the target (index i = T). This semi-empirical cumulative distribution is proven to be accurate for normal and oblique impact of chunky tungsten fragments on steel and aluminum targets at hypervelocity (4 - 7 km/s).
The spatial distribution is assumed to be normal with a standard deviation of 1.1 and an average value of 2. The number of particles in a certain emission angle segment $H_\theta$ can thus be obtained with:

$$H_\theta = \frac{\Delta\theta}{\theta_{max,i}} \frac{5N_i}{1.0582\sqrt{2\pi}} e^{-0.5\left(\frac{5\theta/\theta_{max,i} - 2}{1.1}\right)^2} \tag{8}$$

Here $\Delta\theta$ is the emission angle segment chosen at the characterisation of the data from the witness packs (here 5°).
Figure 11 presents a graphical representation of the distribution of equation (8). Here the emission angle is normalized by the maximum emission angle and the number of fragments by the total amount of fragments.

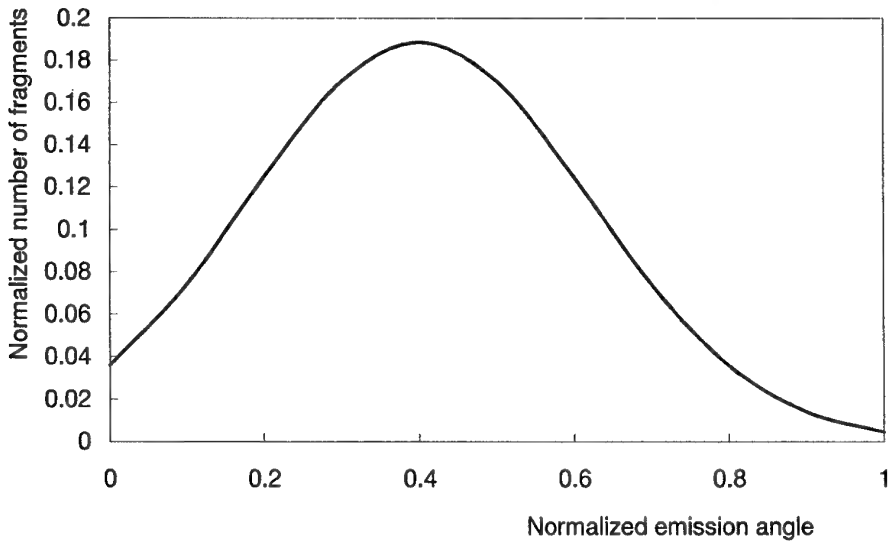


*Figure 11: Normal aerial fragment distribution.*

Notice that in this approach the largest number of fragments are found at an angle of 40% of the maximum emission angle.

For normal impact, the maximum emission angle can be found with the following relation (which represents the experimental data best) [2]:

$$\theta_{max} = 72.9\left(\frac{V_i}{C_T}\right) + 107 \tag{9}$$

**Velocity distribution**

A validated equation for the spatial velocity distribution was already presented in [2]. The projectile is being decelerated by the interaction with the target. The difference in velocity before and after interaction can be obtained from Newton's law of conservation of momentum:

$$V_i - V_l = \frac{\rho_T A_p}{2 M_p} t_T V_i + \frac{R A_p t_T}{V_i M_p} \tag{10}$$

where $A_p$ projected geometrical area of the projectile
R parameter determining the resistance of the target.

In most cases R is approximated by thrice the yield stress Y of the target material. Equation (10) determines the cloud frontal velocity ($V_1$ from Figure 9). The velocity distribution as a function of the emission angle $\theta$ (see Figure 9) follows from the following semi-empirical equation:

$$V_x(\theta) = V_l \cos(1.92\theta) \tag{11}$$

With the above equations, a full theoretical distribution of the debris cloud is finished.

# 4 Hydrocode simulations

AUTODYN-2D is a computercode specifically designed for non-linear dynamic problems. Such codes are often referred to as hydrocodes. The Lagrange processor is particularly efficient in simulating impact problems. In Lagrange the grid distorts with the material and gives good definition of material interfaces even after large deformations have taken place. The performance of Lagrange can even be enhanced by the use of an erosion algorithm. This algorithm works by removing Lagrangian zones which have reached a user-specified strain, typically above 150%. The Lagrange/erosion option has been used succesfully before to simulate hypervelocity impact and the characteristics of the debris cloud [5].
In the simulations presented below the tungsten normal-impact experiments of Table 2 have been studied. Only Lagrange analyses have been performed; it is intended to conduct other simulations with for instance the gridless Smooth Particle Hydrodynamics (SPH) technique at a later stage.
The material models used for both projectile and target material were a Johnson-Cook strength model. The equation of state of RHA was assumed to be linear and the tungsten alloy was assumed to obey a shock equation of state. A minimum tensile pressure cut-off was used to simulate spalling. The values for this tensile limit were found in [6]. Material input data was standard AUTODYN library data, and is given below in Table 9.

*Table 9: Input data for AUTODYN-2D simulations.*

| Material | 4340 Steel | Tungsten Alloy |
|---|---|---|
| Equation of State | Linear | Shock |
| Strength Model | Johnson-Cook | Johnson-Cook |
| Failure Model | Hydro. Tens. Limit | Hydro. Tens. Limit |
| Erosion Model | Inst. Geom. Strain | Inst. Geom. Strain |
| Ref. Density (g/cm$^3$) | 7.83 | 17.8 |
| Bulk Modulus (kPa) | 1.59 E8 | - |
| Ref. Temp. (K) | 300 | 300 |
| Spec. Heat (J/kgK) | 477 | 134 |
| Shear Mod. (kPa) | 8.18 E7 | 16.0 E7 |
| Yield Stress (kPa) | 2.0 E6 | 1.18 E6 |
| Hard. Const (kPa) | 5.1 E5 | 1.77 E5 |
| Hard. Exp. (-) | 0.26 | 0.12 |
| Strain Rate Const. (-) | 0.014 | 0.016 |
| Therm. Soft. Exp. (-) | 1.03 | 1 |
| Melt. Temp. (K) | 1794 | 1723 |
| Parameter C1 (m/s) | - | 4890 |
| Parameter S1 (-) | - | 1.237 |
| Gruneisen Coeff. (-) | - | 1.54 |
| Hydro. Tens. Limit (kPa) | 1.2 E6 | 1.76 E6 |
| Erosion Strain (-) | 1.5 | 2.5 |

The projectile was assumed to have no yaw, in other words the velocity vector and the projectile longitudinal axis were aligned. This allowed a 2D analysis of the problem. Both projectile and target consisted of 1 mm square cells. The target was 5 times the lateral dimension of the projectile (i.e. 30 mm in diameter). This rather coarse grid gives results in good agreement with the experiments. An erosion algorithm was used to remove zones with high deformation, with the nodes being retained as translating mass points after erosion. A plot of the grids during the simulation of a problem is given below as Figure 12.

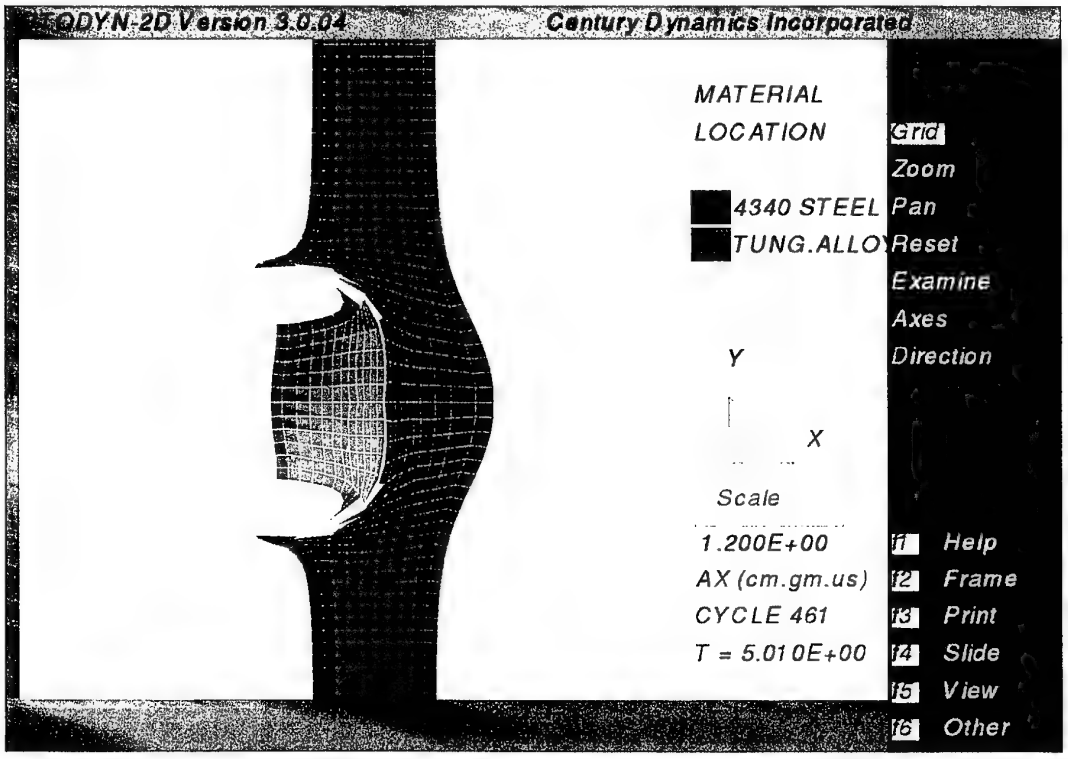


*Figure 12: AUTODYN-2D plot of tungsten cylinder penetrating RHA.*

From the simulations a number of characteristics could be obtained:

- target hole diameter;
- cloud frontal velocity;
- maximum emission angle;
- expansion (lateral) velocities for projectile and target.

Figure 13 shows an example plot after full development of the debris cloud. The eroded nodes can be seen as well as the velocity vectors. The target hole diameter is taken as the inner diameter of non-eroded nodes. The maximum emission angle, rounded to the nearest highest multiple of 5, is obtained from the eroded node with the largest lateral coordinate. The two velocities in axial and lateral direction determine the emission angle. Likewise, the expansion velocity is the lateral velocity of the eroded node at the greatest distance from the line of fire. The latter procedure can be performed for both projectile and target.

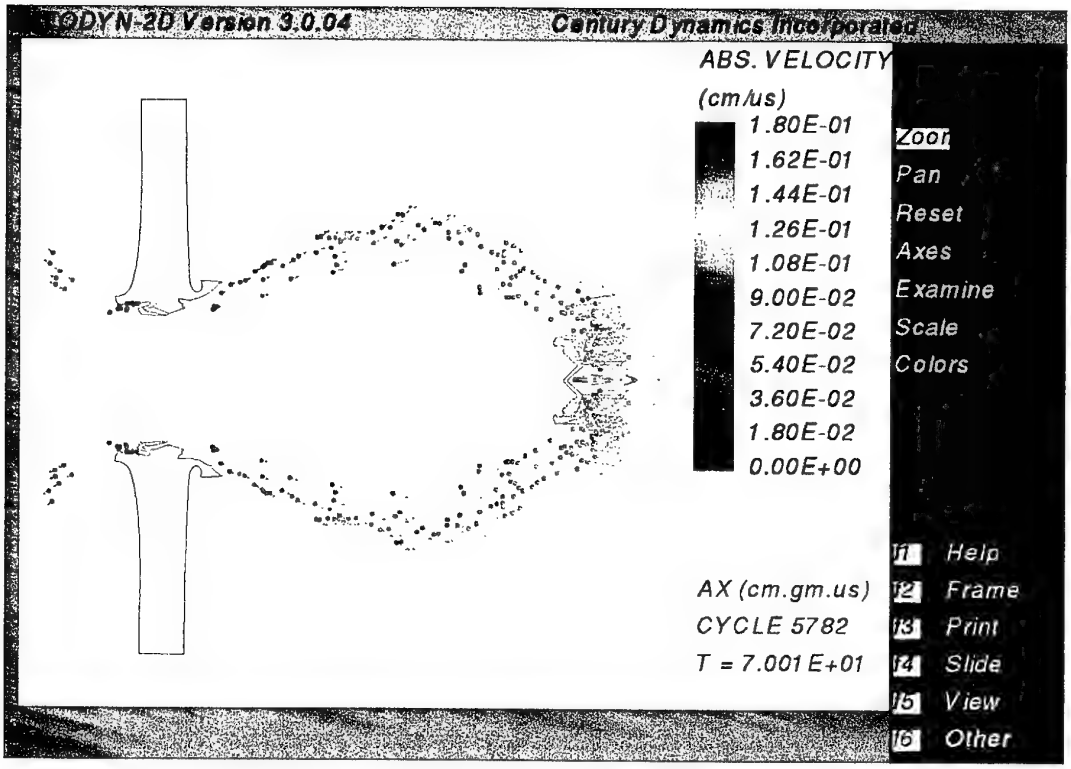


*Figure 13: AUTODYN-2D plot of tungsten cylinder which perforated RHA.*

Table 10 presents the results of the simulations.

*Table 10: Results of AUTODYN-2D simulations for normal impact.*

| Code | D (mm) | $V_1$ (m/s) | $\theta_{max}$ (°) | $V_{yp}$ (m/s) | $V_{yT}$ (m/s) |
|---|---|---|---|---|---|
| T10/1449 | 23±1.5 | 1010 | 30 | 231 | 332 |
| T10/1514 | 23±1.5 | 1078 | 40 | 240 | 378 |
| T10/1779 | 26±1.5 | 1371 | 35 | 330 | 436 |
| T10/1885 | 30±1.5 | 1478 | 35 | 357 | 452 |
| T10/2444 | 30±1.5 | 2116 | 30 | 422 | 553 |
| T20/1525 | 24±1.5 | 1015 | 30 | 109 | 295 |

Notice that there are no trends visible in the maximum emission angle versus the impact velocity. This is caused by the fact that erosion is used to model fragmentation. Here the erosion parameter was tuned to obtain an accurate cloud frontal velocity. It does not have to result in a good spatial distribution. There is some evidence that using the SPH-technique may increase the accuracy of the calculations for this purpose.

# 5 Correlation between model and experiments

The correlation between the experimental results of Chapter 2 and the model and simulations presented in Chapters 3 and 4 respectively can be checked fully for tungsten cylinders only. Unfortunately, no hydrocode simulations of the steel impact cases could be performed due to the unknown projectile material properties Furthermore, the material chosen for the steel projectile was unfortunately inappropriate for fragmentation studies, as already apparent in Chapter 2. The steel was a low-alloyed tool steel (1% C, 0.2 Si and 0.35% Mn) which was surface-hardened. This is a very ductile material (apart from a very thin hardened top-layer) which merely erodes rather than fragments at high-velocity interactions. The results of for instance the multiple-plate impact experiments (Table 6) show that not only very few debris particles are generated by the high-velocity (e.g. 2420 m/s) interaction of steel and RHA but also the penetrative capacity, even of the fragment itself, is disappointing. This proves that the fragment does not break-up, but erodes by the interaction. This behaviour is completely the opposite to the behaviour of tungsten.
In Table 12 the correlation between experimental and calculated characteristics is given. The material properties are listed in Table 11.

*Table 11: Material properties for tungsten alloy and RHA.*

| Material | RHA | Tungsten alloy |
|---|---|---|
| density (g/cm$^3$) | 7.83 | 17.8 |
| yield stress (GPa) | 2.00 | 1.18 |
| $K_{Ic}$ (MPa$\sqrt{m}$) | 40 | 20 |
| C (m/s) | 4610 | 4890 |

With these material properties a scatter coefficient of 0.36 leads to a scatter velocity of approximately 1200 m/s. This correlates rather well with the experimental findings. Up to 1178 m/s only one big hole was found in the witness pack indicating that the tungsten fragment did not break up.
In Table 12 the agreement between the experiments and the simulations/ model is presented. Here the target hole size D, the cloud frontal velocity $V_1$, and the maximum emission angles $\theta_m$ are compared.

*Table 12: Comparison between experimental values and model/simulations.*

| Code | $V_1$ (m/s) exp. | sim. | pred. | $D_{eq}$ (mm) exp. | sim. | pred. | $\theta_m$ (°) exp. | sim. | pred. |
|---|---|---|---|---|---|---|---|---|---|
| T10/1449 | 1064 | 1010 | 1066 | 22 | 23 | 22 | 30 | 30 | 35 |
| T10/1514 | 1154 | 1078 | 1129 | 22 | 23 | 23 | 35 | 40 | 35 |
| T10/1779 | 1368 | 1371 | 1376 | 26 | 26 | 25 | 40 | 35 | 40 |
| T10/1885 | 1475 | 1478 | 1474 | 28 | 30 | 26 | 35 | 35 | 40 |
| T10/2444 | - | 2116 | 1976 | 30 | 30 | 31 | 50 | 30 | 50 |
| T20/1525 | - | 1015 | 783 | 27 | 24 | 23 | 40 | 30 | 35 |
| S10/1477 | - | - | 1103 | 22 | - | 23 | 35 | - | 35 |
| S10/2419 | - | - | 1967 | 30 | - | 30 | 50 | - | 50 |

exp. = experimental.

sim. = AUTODYN simulation.

pred. = prediction with semi-empirical formulas from Chapter 3.

Both the AUTODYN-2D simulations and the semi-empirical model give accurate results. Like stated before, for the maximum emission angle AUTODYN yields less accurate predictions. In the predictions of the damage of the witness pack plates however the semi-empirical methods are used (except for the expansion velocities).

The emission angles are assumed equal for both projectile and target material. The calculation procedure is as follows.

- With the method presented in Chapter 2, the number of holes in the first witness pack plate can be estimated. The total number of particles follows from equations (7).
- It is however obvious that not every particle creates a hole that can be found. First there is for every velocity a certain mass which can just penetrate the first plate of the witness pack. A particle with a lower mass will not create a hole. Second there is the resolution of the camera used to digitize the witness pack plates. It is anticipated here that the second effect determines the cut-off value for the mass of the minimum particle which can be detected. Knowing the number of particles and the maximum emission angle, the distribution function (7) determines the number of particles of each fragmentation mechanism (target and projectile) in each emission angle segment. Here a segment width of 5° is used in compliance with the presentation of the experimental data.
- The resolution in this configuration of the CCD camera is 2 mm. This means that every fragment larger than 2 mm in diameter will create a hole. Filling in this mass in the distribution function (7) will deliver a number of holes in the first witness plate.
- At high velocities the hole can grow larger than the diameter of the projectile. This means that fragments with a diameter smaller than 2 mm can still create a hole of 2 mm. For tungsten fragments impacting 0.8 mm aluminium the following simple relation is found [3]:

$$\frac{D}{d}=1+\left(1.5V^{2/3}-1\right)\left(1-e^{-3t/d}\right) \tag{12}$$

In this equation D is the hole size in a plate with thickness t formed by the impact at a velocity V of a projectile with diameter d. In steel the hole growth as a function of the velocity is totally unknown and needs to be studied.

With this procedure an estimate for the total number of holes can be found. The steel projectiles did not fragment. They were assumed to cause only one hole. The expansion velocity could not be obtained and was chosen to be equal to the equivalent for tungsten (for 1477 m/s, 332 m/s and for 2419 m/s. 533 m/s). In Table 13 the estimated values are compared to the experimental, where a lower-bound is given for no hole growth. The upperbound is the value found when hole growth is taken into account by means of equation (12).

*Table 13: A comparison between the estimated number of holes in the first witness pack plate and the experimental values.*

| Code | Exp. | Pred. (no growth) | Pred. (hole growth) |
|---|---|---|---|
| T10/1449 | 270 | 216 | 435 |
| T10/1514 | 336 | 248 | 507 |
| T10/1779 | 529 | 290 | 762 |
| T10/1885 | 600 | 311 | 901 |
| T10/2444 | 802 | 467 | 1564 |
| T20/1525 | 83 | 307 | 337 |
| S10/1477 | 38 | 124 | 145 |
| S10/2419 | 357 | 388 | 672 |

The worst results are obtained for steel. This is probably caused by the cloud expansion velocity chosen. A slight change in expansion velocity (= average fragment size) causes a big difference in hole count. For example, changing the expansion velocity for the S10/1477 experiment from 332 m/s to 200 m/s leads to a hole count with no hole growth of 64. This correlates somewhat better to the experimental result.

For tungsten the experimental values for the hole count are in between the no-growth and the hole growth value, except for the experiment at 20 mm RHA. As the velocity increases, the values tend towards the hole growth values. This makes sense, because at a higher velocity also the fragment velocity is higher and consequently also hole growth becomes more significant. Due to the fact that the method used to compensate for hole growth is developed purely for aluminium, the correlation for steel is rather poor. Steel is less ductile than aluminium. Thus hole growth in steel will lie somewhere inbetween the no-growth value and the value for hole growth in aluminium.

The prediction for 20 mm RHA appears completely wrong. There are however some effects, unique for the 20 mm RHA, which can influence the prediction significantly:

- the cloud frontal velocity is lowest for this experiment. This could mean that not the visual criterion of the smallest detectable hole but the penetration relation for the first witness pack plate becomes dominant;
- the overmatch (the ratio of residual velocity and perforation threshold velocity) is lowest for this experiment, which could have a large effect on the energy delivered to create spallation;
- there could be a completely different dominant mechanism for 20 mm RHA as apposed to 10 mm. Because this is the only experiment with 20 mm of RHA no conclusion can be drawn. One can imagine for example that for a 20 mm plate much more (percentage wise) material is thrown off to the entrance side of the armour.

It is obvious that more work should be done to understand the apparently totally different behaviour of the 20 mm RHA plate.

Up to now only the damage inflicted to the first plate of the witness pack can be estimated, taking into account only the visual detectability of the holes. More work should be done to generate perforation threshold curves for all plates. Such a curve determines as a function of the velocity and the mass of a fragment the penetrative capacity into a witness pack.

The spatial distribution of the fragments as a function of the emission angle can be predicted rather well. Figure 14 gives the correlation between the predictions and the experimental values for the T10/1449 and the T10/2444 experiments.

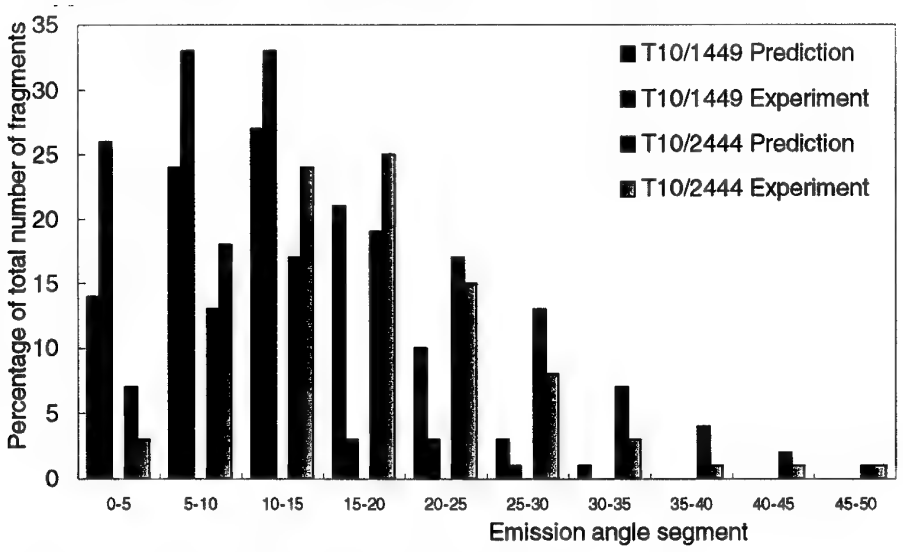


*Figure 14: Spatial distributions of fragments.*

Considering the complexity of fragmentation the distributions are rather well predicted. The prediction for the highest velocity is more accurate than for the low velocity.

**Evaluation**

The model based on a combination of semi-empirical relations and hydrocode simulations is capable of modeling the behind armour debris for normal impact of tungsten cylinders. It can predict the target plate hole size, the velocity distribution and the spatial distribution of fragments (number and mass) inside a debris cloud. With some assumed simple empirical relations the number of holes in the first witness pack plate can be determined with a reasonable accuracy. The experimental value is for the thin plates always within a bandwidth of predictions assuming on the one hand no hole growth and on the other hand hole growth in aluminium plates. For thicker target plates the prediction of the number of holes is rather poor for yet unknown reasons.

# 6 Conclusions

This report is the third report in a series describing the development of a fragmentation model for behind armour debris originating from fragmentation of projectiles and target plates due to high-velocity impact interactions. This model is a combination of semi-empirical laws, validated by carefully-conducted experiments, and hydrocode simulations. The model is capable of predicting:

- the target hole diameter;
- the velocity distribution in the debris cloud;
- the maximum emission angle of the fragments;
- the spatial distribution i.e, number of fragments and mass as a function of the emission angle.

A first estimate to predict the projectile impact velocity at which full scattering of the fragment occurs is also presented. This method gives useful results but should be used with great caution due to the assumptions made.

The number of perforations found in the first witness pack plate lies always within the lower- and upperbound predictions with the model presented here. The lowerbound of the predictions is given by the visually detectable number of holes, where no hole growth after perforation is assumed. For an upperbound prediction a semi-empirical method is used which predicts (for thin aluminium plates) the hole growth as a function of the impact velocity and the mass of the impactor.

From the experiments it is found that as the impact velocity increases:

- the number of fragments increases;
- the average fragment size decreases;
- the penetrative capability decreases;
- the size of the perforated hole in the target increases.

The tungsten fragment breaks up at the interaction with RHA above an impact velocity of approximately 1200 m/s. The behind-armour debris cloud disperses considerably (cone apex angle of maximum 50 degrees) and is capable of penetrating a number of plates. For example, the multiple plate target representing an armoured helicopter is fully penetrated. The material for the steel fragment chosen here was capable of penetrating only two plates of the same multiple plate target at equal velocity. The steel, as opposed to the tungsten, did not break-up and was as a consequence less effective.

All above conclusions are based on a limited number of experiments.

# 7 Recommendations

In the remainder of the project attention should be focussed on:

- *modern aircraft materials*, like aluminium. Based on a scatter parameter of 0.36, the necessary velocity to completely shatter tungsten by impacting aluminium is 1.5 km/s. This velocity can be reached easily experimentally;
- checking the semi-empirical relation for the *mass distribution*. This can be done by performing impact experiments and soft-catching the debris instead of witness packs. This allows a determination of the mass and the number of fragments;
- determining a correct *hole growth equation* for thin steel;
- *calibrate* the all-steel *witness pack*. This means determining the perforation threshold curves, the velocity at which a fragment with a certain mass is capable of perforating a certain amount of plates;
- perform more *AUTODYN simulations* to find the influence of yaw, oblique impact, and the SPH-method;
- expand the model to include *oblique impact*.

# 8 References

1 Ingen, R.P. van,
'Inslag van hoge-snelheidsfragmenten op luchtdoelen: een verkennende studie',
TNO-rapport PML 1996-A14, juni 1996.

2 Verolme, J.L.,
'Inslag van hoge-snelheidsfragmenten op luchtdoelen. 'Behind Armour Debris' modellering en oriënterende experimenten'
TNO-rapport PML 1997-A4, april 1997.

3 Ari, N. and Wilbeck, J.S.,
'Debris Fragment Characterisation in Oblique Hypervelocity Impacts',
Int. J. Impact Eng. Vol. 14, pp 37-48, 1993.

4 Kipp, M.E. et al.,
'Experimental and numerical studies of high-velocity impact fragmentation',
SANDIA Report SAND93-0773.UC-410, Albuquerque, New Mexico, USA, augustus 1993.

5 Hayhurst, C.J. and Clegg, R.C.,
'Cylindrically symmetric SPH simulations of hypervelocity impacts on thin plates',
1996 HVIS symposium, Freiburg, Germany, to be published Int. J. Impact Eng. 1997.

6 Chhabildas, L.C. and Barker, L.M.,
'Relationship of fragment size to normalized spall strength for materials',
Int. J. Impact Eng. Vol. 10, pp 107-124, 1990.

# 9 Authentication

J.L.M.J. van Bree
Research Co-ordinator

Dr. J.L. Verolme
Project leader/Author

# Annex A Normal and oblique impact

## Normal impact

Experiment **3556**

Projectile **Tungsten**

Target **RHA 10mm**

Velocity (m/s) **1449**

| Emission Angle Segment (°) | Number of Perforations in Plate | | | | | |
|---|---|---|---|---|---|---|
| | 1 | 2 | 3 | 4 | 5 | 6 |
| 0-5 | 71 | 34 | 19 | 2 | | |
| 5-10 | 88 | 21 | 3 | 1 | | |
| 10-15 | 89 | 9 | 0 | 0 | | |
| 15-20 | 9 | 0 | 0 | 0 | | |
| 20-25 | 8 | 0 | 0 | 0 | | |
| 25-30 | 4 | 1 | 0 | 0 | | |
| 30-35 | 0 | 0 | 0 | 0 | | |
| 35-40 | 1 | 0 | 0 | 0 | | |
| 40-45 | 0 | 0 | 0 | 0 | | |
| 45-50 | | | | | | |

| Area Class ($mm^2$) | Number of Holes per Area Class in Plate | | | | | |
|---|---|---|---|---|---|---|
| | 1 | 2 | 3 | 4 | 5 | 6 |
| 0-10 | 225 | 43 | 9 | 0 | | |
| 10-25 | 21 | 15 | [illegible] | 2 | | |
| 25-50 | 9 | 2 | 3 | 1 | | |
| 50-100 | 8 | 2 | 1 | | | |
| 100-250 | 7 | 2 | 3 | | | |
| 250-500 | | 1 | 1 | | | |
| 500-1000 | | | | | | |
| Total | 270 | 65 | 22 | 3 | 0 | 0 |

Experiment **3553**

Projectile **Tungsten**

Target **RHA 10mm**

Velocity (m/s) **1514**

| Emission Angle Segment (°) | Number of Perforations in Plate | | | | | |
|---|---|---|---|---|---|---|
| | 1 | 2 | 3 | 4 | 5 | 6 |
| 0-5 | 92 | 38 | 14 | 3 | | |
| 5-10 | 114 | 41 | 13 | 0 | | |
| 10-15 | 86 | 9 | 1 | 0 | | |
| 15-20 | 33 | 0 | 0 | 0 | | |
| 20-25 | 1 | 0 | 0 | 0 | | |
| 25-30 | 8 | 0 | 0 | | | |
| 30-35 | 2 | 0 | 0 | | | |
| 35-40 | 0 | 0 | 0 | | | |
| 40-45 | 0 | 0 | 0 | | | |
| 45-50 | 0 | | | | | |

| Area Class ($mm^2$) | Number of Holes per Area Class in Plate | | | | | |
|---|---|---|---|---|---|---|
| | 1 | 2 | 3 | 4 | 5 | 6 |
| 0-10 | 273 | 57 | 14 | 2 | | |
| 10-25 | 33 | 15 | 6 | 1 | | |
| 25-50 | 17 | 9 | 4 | | | |
| 50-100 | 8 | 7 | 2 | | | |
| 100-250 | 4 | | 2 | | | |
| 250-500 | 1 | | | | | |
| 500-1000 | | | | | | |
| Total | 336 | 88 | 28 | 3 | 0 | 0 |

Experiment
**3555**

Projectile
Tungsten

Target
RHA 10mm

Velocity (m/s)
1779

| Emission Angle Segment (°) | Number of Perforations in Plate | | | | | |
|---|---|---|---|---|---|---|
| | 1 | 2 | 3 | 4 | 5 | 6 |
| 0-5 | 95 | 30 | 11 | 3 | | |
| 5-10 | 150 | 47 | 16 | 2 | | |
| 10-15 | 124 | 25 | 3 | 0 | | |
| 15-20 | 115 | 2 | 0 | 0 | | |
| 20-25 | 23 | 1 | 0 | 0 | | |
| 25-30 | 10 | 1 | 0 | 0 | | |
| 30-35 | 5 | 0 | 0 | 0 | | |
| 35-40 | 7 | 0 | 0 | 0 | | |
| 40-45 | 0 | 0 | 0 | 0 | | |
| 45-50 | | | | | | |

| Area Class ($mm^2$) | Number of Holes per Area Class in Plate | | | | | |
|---|---|---|---|---|---|---|
| | 1 | 2 | 3 | 4 | 5 | 6 |
| 0-10 | 459 | 79 | 18 | 4 | | |
| 10-25 | 35 | 12 | 3 | 1 | | |
| 25-50 | 21 | 9 | 2 | | | |
| 50-100 | 8 | 4 | 6 | | | |
| 100-250 | 5 | 1 | 1 | | | |
| 250-500 | 1 | 0 | | | | |
| 500-1000 | | 1 | | | | |
| Total | 529 | 106 | 30 | 5 | 0 | 0 |

Experiment
**3552**

Projectile
Tungsten

Target
RHA 10mm

Velocity (m/s)
1885

| Emission Angle Segment (°) | Number of Perforations in Plate | | | | | |
|---|---|---|---|---|---|---|
| | 1 | 2 | 3 | 4 | 5 | 6 |
| 0-5 | 101 | 32 | 16 | | | |
| 5-10 | 169 | 59 | 17 | | | |
| 10-15 | 139 | 37 | 1 | | | |
| 15-20 | 135 | 2 | 1 | | | |
| 20-25 | 36 | 1 | 0 | | | |
| 25-30 | 6 | 0 | 0 | | | |
| 30-35 | 7 | 0 | 0 | | | |
| 35-40 | 7 | 0 | 0 | | | |
| 40-45 | 0 | 0 | 0 | | | |
| 45-50 | | | | | | |

| Area Class ($mm^2$) | Number of Holes per Area Class in Plate | | | | | |
|---|---|---|---|---|---|---|
| | 1 | 2 | 3 | 4 | 5 | 6 |
| 0-10 | 519 | 95 | 24 | | | |
| 10-25 | 48 | 13 | 5 | | | |
| 25-50 | 20 | 15 | 5 | | | |
| 50-100 | 9 | 6 | 1 | | | |
| 100-250 | 4 | 1 | | | | |
| 250-500 | | 1 | | | | |
| 500-1000 | | | | | | |
| Total | 600 | 131 | 35 | 0 | 0 | 0 |

Experiment **3857**

Projectile **Tungsten**

Target **RHA 10 mm**

Velocity (m/s) **2444**

| Emission Angle Segment (°) | Number of Perforations in Plate | | | | | |
|---|---|---|---|---|---|---|
| | 1 | 2 | 3 | 4 | 5 | 6 |
| 0-5 | 27 | 11 | 8 | | | |
| 5-10 | 145 | 52 | 13 | | | |
| 10-15 | 191 | 30 | 1 | | | |
| 15-20 | 203 | 11 | 0 | | | |
| 20-25 | 121 | 1 | 0 | | | |
| 25-30 | 66 | 4 | 0 | | | |
| 30-35 | 25 | 2 | 0 | | | |
| 35-40 | 10 | 0 | 0 | | | |
| 40-45 | 5 | 0 | 0 | | | |
| 45-50 | 9 | 0 | | | | |

| Area Class ($mm^2$) | Number of Holes per Area Class in Plate | | | | | |
|---|---|---|---|---|---|---|
| | 1 | 2 | 3 | 4 | 5 | 6 |
| 0-10 | 695 | 86 | 14 | | | |
| 10-25 | 62 | 12 | 2 | | | |
| 25-50 | 35 | 5 | 2 | | | |
| 50-100 | 5 | 6 | 3 | | | |
| 100-250 | 3 | 1 | 1 | | | |
| 250-500 | 1 | 0 | | | | |
| 500-1000 | 0 | 0 | | | | |
| 1000-2500 | 1 | 0 | | | | |
| 2500-5000 | | 1 | | | | |
| Total | 802 | 111 | 22 | 0 | 0 | 0 |

Experiment **3856**

Projectile **Tungsten**

Target **RHA 20mm**

Velocity (m/s) **1525**

| Emission Angle Segment (°) | Number of Perforations in Plate | | | | | |
|---|---|---|---|---|---|---|
| | 1 | 2 | 3 | 4 | 5 | 6 |
| 0-5 | 24 | 4 | 2 | 1 | | |
| 5-10 | 37 | 8 | 2 | 0 | | |
| 10-15 | 14 | 3 | 0 | 0 | | |
| 15-20 | 3 | 1 | 0 | 0 | | |
| 20-25 | 1 | 0 | 0 | | | |
| 25-30 | 1 | 0 | 0 | | | |
| 30-35 | 2 | 0 | 0 | | | |
| 35-40 | 1 | 0 | | | | |
| 40-45 | | | | | | |
| 45-50 | | | | | | |

| Area Class ($mm^2$) | Number of Holes per Area Class in Plate | | | | | |
|---|---|---|---|---|---|---|
| | 1 | 2 | 3 | 4 | 5 | 6 |
| 0-10 | 59 | 7 | 1 | 1 | | |
| 10-25 | 4 | 2 | 0 | | | |
| 25-50 | 4 | 0 | 0 | | | |
| 50-100 | 4 | 2 | 0 | | | |
| 100-250 | 5 | 4 | 3 | | | |
| 250-500 | 6 | 1 | | | | |
| 500-1000 | 1 | | | | | |
| Total | 83 | 16 | 4 | 1 | 0 | 0 |

Experiment
**3855**

Projectile
**Steel**

Target
**RHA 10mm**

Velocity (m/s)
**1477**

| Emission Angle Segment ($^0$) | Number of Perforations in Plate | | | | | |
|---|---|---|---|---|---|---|
| | 1 | 2 | 3 | 4 | 5 | 6 |
| 0-5 | 13 | 1 | 0 | | | |
| 5-10 | 19 | 1 | 1 | | | |
| 10-15 | 5 | 0 | 0 | | | |
| 15-20 | 0 | 0 | 0 | | | |
| 20-25 | 0 | 0 | | | | |
| 25-30 | 0 | | | | | |
| 30-35 | 1 | | | | | |
| 35-40 | 0 | | | | | |
| 40-45 | | | | | | |
| 45-50 | | | | | | |

| Area Class ($mm^2$) | Number of Holes per Area Class in Plate | | | | | |
|---|---|---|---|---|---|---|
| | 1 | 2 | 3 | 4 | 5 | 6 |
| 0-10 | 20 | 1 | 0 | | | |
| 10-25 | 5 | 1 | 0 | | | |
| 25-50 | 3 | | 0 | | | |
| 50-100 | 3 | | 0 | | | |
| 100-250 | 6 | | 0 | | | |
| 250-500 | 1 | | 1 | | | |
| 500-1000 | | | | | | |
| Total | 38 | 2 | 1 | 0 | 0 | 0 |

Experiment
**3858**

Projectile
**Steel**

Target
**RHA 10mm**

Velocity (m/s)
**2419**

| Emission Angle Segment ($^0$) | Number of Perforations in Plate | | | | | |
|---|---|---|---|---|---|---|
| | 1 | 2 | 3 | 4 | 5 | 6 |
| 0-5 | 40 | 3 | 0 | | | |
| 5-10 | 90 | 7 | 1 | | | |
| 10-15 | 108 | 5 | 0 | | | |
| 15-20 | 61 | 2 | 0 | | | |
| 20-25 | 27 | 0 | 0 | | | |
| 25-30 | 13 | 1 | 0 | | | |
| 30-35 | 6 | 0 | 0 | | | |
| 35-40 | 8 | 1 | | | | |
| 40-45 | 2 | 0 | | | | |
| 45-50 | 1 | 0 | | | | |

| Area Class ($mm^2$) | Number of Holes per Area Class in Plate | | | | | |
|---|---|---|---|---|---|---|
| | 1 | 2 | 3 | 4 | 5 | 6 |
| 0-10 | 278 | 7 | 0 | | | |
| 10-25 | 35 | 6 | 1 | | | |
| 25-50 | 20 | 5 | | | | |
| 50-100 | 20 | 1 | | | | |
| 100-250 | 4 | | | | | |
| 250-500 | | | | | | |
| 500-1000 | | | | | | |
| Total | 356 | 19 | 1 | 0 | 0 | 0 |

# Oblique impact

Experiment: 3860
Projectile: Tungsten
Target: RHA 10mm
Velocity (m/s): 2438
Angle of Obliquity (°): 30

| Emission Angle | Number of Perforations per Sector | | | | | | | | | | | | | | | |
|---|---|---|---|---|---|---|---|---|---|---|---|---|---|---|---|---|
| | Plate 1 | | | | Plate 2 | | | | Plate 3 | | | | Plate 4 | | | |
| Segment (°) | 0-45 | 45-90 | 90-135 | 135-180 | 0-45 | 45-90 | 90-135 | 135-180 | 0-45 | 45-90 | 90-135 | 135-180 | 0-45 | 45-90 | 90-135 | 135-180 |
| 0-5 | 8 | 6 | 6 | 6 | 2 | 0 | 1 | 1 | 2 | 0 | 0 | 0 | 0 | 0 | 0 | 0 |
| 5-10 | 13 | 16 | 16 | 25 | 2 | 2 | 6 | 10 | 0 | 0 | 0 | 3 | 0 | 0 | 0 | 0 |
| 10-15 | 25 | 31 | 39 | 45 | 4 | 1 | 5 | 15 | 0 | 0 | 1 | 9 | 0 | 0 | 0 | 2 |
| 15-20 | 7 | 25 | 34 | 63 | 2 | 3 | 3 | 29 | 0 | 1 | 0 | 12 | 0 | 0 | 0 | 0 |
| 20-25 | 13 | 5 | 41 | 93 | 1 | 0 | 2 | 17 | 0 | 0 | 0 | 1 | 0 | 0 | 0 | 0 |
| 25-30 | 9 | 6 | 23 | 68 | 1 | 1 | 2 | 4 | 0 | 0 | 0 | 0 | 0 | 0 | 0 | 0 |
| 30-35 | 9 | 5 | 6 | 14 | 1 | 0 | 1 | 0 | 0 | 0 | 0 | 0 | 0 | 0 | 0 | 0 |
| 35-40 | 5 | 2 | 11 | 4 | 0 | 0 | 0 | 0 | 0 | 0 | 0 | 0 | 0 | 0 | 0 | 0 |
| 40-45 | 1 | 5 | 0 | 0 | 0 | 0 | 0 | 0 | 0 | 0 | 0 | 0 | 0 | 0 | 0 | 0 |
| 45-50 | 0 | 1 | 0 | 0 | 0 | 0 | 0 | 0 | 0 | 0 | 0 | 0 | 0 | 0 | 0 | 0 |

| Area | Number of Holes per Area Class in Sector | | | | | | | | | | | | | | | |
|---|---|---|---|---|---|---|---|---|---|---|---|---|---|---|---|---|
| | Plate 1 | | | | Plate 2 | | | | Plate 3 | | | | Plate 4 | | | |
| Class (mm²) | 0-45 | 45-90 | 90-135 | 135-180 | 0-45 | 45-90 | 90-135 | 135-180 | 0-45 | 45-90 | 90-135 | 135-180 | 0-45 | 45-90 | 90-135 | 135-180 |
| 0-10 | 70 | 85 | 155 | 265 | 5 | 2 | 16 | 53 | 1 | 0 | 1 | 17 | 0 | 0 | 0 | 1 |
| 10-25 | 8 | 11 | 12 | 34 | 3 | 3 | 3 | 5 | 0 | 1 | 0 | 2 | 0 | 0 | 0 | 1 |
| 25-50 | 9 | 5 | 6 | 9 | 3 | 2 | 1 | 10 | 0 | 0 | 0 | 2 | | | | |
| 50-100 | 3 | 4 | 3 | 8 | 2 | 0 | 0 | 6 | 1 | 0 | 0 | 1 | | | | |
| 100-250 | 0 | 1 | 0 | 1 | 0 | 0 | 0 | 1 | 0 | 0 | 0 | 2 | | | | |
| 250-500 | 0 | 0 | 0 | 1 | 0 | 0 | 0 | 1 | 0 | 0 | 0 | 1 | | | | |
| 500-1000 | | | | | | | | | | | | | | | | |
| Total | 690 | | | | 116 | | | | 29 | | | | 2 | | | |

Experiment: 3862
Projectile: Tungsten
Target: RHA 10mm
Velocity (m/s): 2416
Angle of Obliquity (°): 60

| Emission Angle | Number of Perforations per Sector | | | | | | | | | | | | | | | |
|---|---|---|---|---|---|---|---|---|---|---|---|---|---|---|---|---|
| | Plate 1 | | | | Plate 2 | | | | Plate 3 | | | | Plate 4 | | | |
| Segment (°) | 0-45 | 45-90 | 90-135 | 135-180 | 0-45 | 45-90 | 90-135 | 135-180 | 0-45 | 45-90 | 90-135 | 135-180 | 0-45 | 45-90 | 90-135 | 135-180 |
| 0-5 | 1 | 2 | 3 | 7 | 0 | 0 | 0 | 0 | 0 | 0 | 0 | 0 | 0 | | | |
| 5-10 | 6 | 5 | 10 | 15 | 1 | 1 | 0 | 1 | 0 | 0 | 0 | 1 | 0 | | | |
| 10-15 | 8 | 2 | 9 | 17 | 2 | 0 | 1 | 1 | 1 | 0 | 0 | 0 | 1 | | | |
| 15-20 | 10 | 7 | 9 | 24 | 4 | 2 | 0 | 2 | 1 | 1 | 0 | 0 | 0 | | | |
| 20-25 | 10 | 5 | 13 | 63 | 3 | 0 | 0 | 14 | 3 | 0 | 0 | 7 | 0 | | | |
| 25-30 | 4 | 6 | 7 | 43 | 2 | 0 | 0 | 8 | 0 | 0 | 0 | 2 | 0 | | | |
| 30-35 | 10 | 7 | 5 | 2 | 4 | 0 | 0 | 0 | 0 | 0 | 0 | 0 | 0 | | | |
| 35-40 | 3 | 2 | 0 | 1 | 0 | 0 | 0 | 0 | 0 | 0 | 0 | 0 | 0 | | | |
| 40-45 | 3 | 1 | 0 | 0 | 1 | 0 | 0 | 0 | 0 | 0 | 0 | 0 | 0 | | | |
| 45-50 | 1 | 0 | 0 | 0 | 0 | 0 | 0 | 0 | 0 | 0 | 0 | 0 | 0 | | | |

| Area | Number of Holes per Area Class in Sector | | | | | | | | | | | | | | | |
|---|---|---|---|---|---|---|---|---|---|---|---|---|---|---|---|---|
| | Plate 1 | | | | Plate 2 | | | | Plate 3 | | | | Plate 4 | | | |
| Class (mm²) | 0-45 | 45-90 | 90-135 | 135-180 | 0-45 | 45-90 | 90-135 | 135-180 | 0-45 | 45-90 | 90-135 | 135-180 | 0-45 | 45-90 | 90-135 | 135-180 |
| 0-10 | 30 | 20 | 48 | 144 | 8 | 0 | 0 | 18 | 0 | 0 | 0 | 6 | 0 | | | |
| 10-25 | 7 | 7 | 5 | 16 | 3 | 1 | 1 | 5 | 2 | 1 | 0 | 3 | 0 | | | |
| 25-50 | 8 | 3 | 2 | 6 | 2 | 2 | 0 | 2 | 1 | 0 | 0 | 1 | 1 | | | |
| 50-100 | 4 | 4 | 1 | 5 | 1 | 0 | 0 | 1 | 0 | 0 | 0 | 0 | | | | |
| 100-250 | 4 | 2 | 0 | 1 | 2 | 0 | 0 | 0 | 1 | 0 | 0 | 0 | | | | |
| 250-500 | 3 | 1 | 0 | 0 | 1 | 0 | 0 | 0 | 1 | 0 | 0 | 0 | | | | |
| 500-1000 | | | | | | | | | | | | | | | | |
| Total | 321 | | | | 47 | | | | 16 | | | | 1 | | | |

Experiment: 3859

Projectile: Steel

Target: RHA 10mm

Velocity (m/s): 1567

Angle of Obliquity (°): 30

| Emission Angle | Number of Perforations per Sector | | | | | | | | | | | |
|---|---|---|---|---|---|---|---|---|---|---|---|---|
| | Plate 1 | | | | Plate 2 | | | | Plate 3 | | | |
| Segment (°) | 0-45 | 45-90 | 90-135 | 135-180 | 0-45 | 45-90 | 90-135 | 135-180 | 0-45 | 45-90 | 90-135 | 135-180 |
| 0-5 | 0 | 1 | 1 | 2 | 0 | 0 | 0 | 0 | 0 | 0 | 0 | 0 |
| 5-10 | 0 | 1 | 1 | 1 | 0 | 1 | 0 | 0 | 0 | 0 | 0 | 0 |
| 10-15 | 2 | 1 | 0 | 2 | 2 | 0 | 0 | 1 | 2 | 0 | 0 | 0 |
| 15-20 | 0 | 0 | 0 | 0 | 0 | 0 | 0 | 0 | 0 | 0 | 0 | 0 |
| 20-25 | 1 | 0 | 0 | 0 | 1 | 0 | 0 | 0 | 0 | 0 | 0 | 0 |
| 25-30 | 0 | 0 | 0 | 0 | 0 | 0 | 0 | 0 | 0 | 0 | 0 | 0 |
| 30-35 | 0 | 0 | 0 | 0 | 0 | 0 | 0 | 0 | 0 | 0 | 0 | 0 |
| 35-40 | 0 | 0 | 0 | 0 | 0 | 0 | 0 | 0 | 0 | 0 | 0 | 0 |
| 40-45 | | | | | | | | | | | | |
| 45-50 | | | | | | | | | | | | |

| Area | Number of Holes per Area Class in Sector | | | | | | | | | | | |
|---|---|---|---|---|---|---|---|---|---|---|---|---|
| | Plate 1 | | | | Plate 2 | | | | Plate 3 | | | |
| Class ($mm^2$) | 0-45 | 45-90 | 90-135 | 135-180 | 0-45 | 45-90 | 90-135 | 135-180 | 0-45 | 45-90 | 90-135 | 135-180 |
| 0-10 | 0 | 1 | 1 | 4 | 0 | 0 | 0 | 1 | 2 | 0 | 0 | 0 |
| 10-25 | 0 | 1 | 1 | 0 | 0 | 0 | 0 | 0 | 0 | 0 | 0 | 0 |
| 25-50 | 0 | 0 | 0 | 0 | 0 | 0 | 0 | 0 | 0 | 0 | 0 | 0 |
| 50-100 | 0 | 0 | 0 | 0 | 0 | 0 | 0 | 0 | 0 | 0 | 0 | 0 |
| 100-250 | 0 | 1 | 0 | 1 | 2 | 1 | 0 | 0 | 0 | 0 | 0 | 0 |
| 250-500 | 3 | 0 | 0 | 0 | 1 | 0 | 0 | 0 | 0 | 0 | 0 | 0 |
| 500-1000 | | | | | | | | | | | | |
| Total | 13 | | | | 5 | | | | 2 | | | |

Experiment: 3861

Projectile: Steel

Target: RHA 10mm

Velocity (m/s): 2396

Angle of Obliquity (°): 30

| Emission Angle | Number of Perforations per Sector | | | | | | | | | | | |
|---|---|---|---|---|---|---|---|---|---|---|---|---|
| | Plate 1 | | | | Plate 2 | | | | Plate 3 | | | |
| Segment (°) | 0-45 | 45-90 | 90-135 | 135-180 | 0-45 | 45-90 | 90-135 | 135-180 | 0-45 | 45-90 | 90-135 | 135-180 |
| 0-5 | 1 | 2 | 1 | 1 | 0 | 0 | 1 | 0 | 0 | 0 | 0 | 0 |
| 5-10 | 2 | 1 | 7 | 13 | 0 | 1 | 0 | 0 | 0 | 0 | 0 | 0 |
| 10-15 | 3 | 0 | 8 | 31 | 0 | 0 | 1 | 2 | 0 | 0 | 0 | 0 |
| 15-20 | 10 | 1 | 6 | 78 | 3 | 0 | 1 | 0 | 1 | 0 | 0 | 0 |
| 20-25 | 6 | 3 | 2 | 13 | 2 | 1 | 0 | 0 | 1 | 0 | 0 | 0 |
| 25-30 | 3 | 2 | 1 | 4 | 0 | 0 | 0 | 1 | 0 | 0 | 0 | 0 |
| 30-35 | 1 | 3 | 3 | 0 | 1 | 0 | 0 | 0 | 0 | 0 | 0 | 0 |
| 35-40 | 2 | 0 | 1 | 0 | 0 | 0 | 0 | 0 | 0 | 0 | 0 | 0 |
| 40-45 | 0 | 0 | 0 | 0 | 0 | 0 | 0 | 0 | 0 | 0 | 0 | 0 |
| 45-50 | 1 | 0 | 0 | 1 | 0 | 0 | 0 | 0 | 0 | 0 | 0 | 0 |

| Area | Number of Holes per Area Class in Sector | | | | | | | | | | | |
|---|---|---|---|---|---|---|---|---|---|---|---|---|
| | Plate 1 | | | | Plate 2 | | | | Plate 3 | | | |
| Class ($mm^2$) | 0-45 | 45-90 | 90-135 | 135-180 | 0-45 | 45-90 | 90-135 | 135-180 | 0-45 | 45-90 | 90-135 | 135-180 |
| 0-10 | 10 | 4 | 21 | 122 | 0 | 0 | 1 | 1 | 0 | 0 | 0 | 0 |
| 10-25 | 2 | 2 | 3 | 11 | 1 | 1 | 0 | 1 | 1 | 0 | 0 | 0 |
| 25-50 | 8 | 1 | 2 | 4 | 2 | 1 | 0 | 0 | 0 | 0 | 0 | 0 |
| 50-100 | 8 | 3 | 2 | 3 | 2 | 0 | 2 | 0 | 1 | 0 | 0 | 0 |
| 100-250 | 1 | 1 | 1 | 1 | 1 | 0 | 0 | 1 | 0 | 0 | 0 | 0 |
| 250-500 | 0 | 1 | 0 | 0 | | | | | 0 | 0 | 0 | 0 |
| 500-1000 | | | | | | | | | 0 | 0 | 0 | 0 |
| Total | 211 | | | | 14 | | | | 2 | | | |

Experiment
3863

Projectile
Steel

Target
RHA 10mm

Velocity (m/s)
2400

Angle of Obliquity (°)
60

| Emission Angle | Number of Perforations per Sector | | | | | | | |
|---|---|---|---|---|---|---|---|---|
| | Plate 1 | | | | Plate 2 | | | |
| Segment (°) | 0-45 | 45-90 | 90-135 | 135-180 | 0-45 | 45-90 | 90-135 | 135-180 |
| 0-5 | 0 | 0 | 0 | 0 | 0 | | | |
| 5-10 | 0 | 0 | 0 | 0 | 0 | | | |
| 10-15 | 0 | 0 | 0 | 0 | 0 | | | |
| 15-20 | 1 | 1 | 0 | 0 | 1 | | | |
| 20-25 | 0 | 0 | 0 | 0 | 0 | | | |
| 25-30 | 0 | 0 | 0 | 0 | 0 | | | |
| 30-35 | 0 | 0 | 0 | 0 | 0 | | | |
| 35-40 | 0 | 0 | 0 | 0 | 0 | | | |
| 40-45 | | | | | | | | |
| 45-50 | | | | | | | | |

| Area | Number of Holes per Area Class in Sector | | | | | | | |
|---|---|---|---|---|---|---|---|---|
| | Plate 1 | | | | Plate 2 | | | |
| Class ($mm^2$) | 0-45 | 45-90 | 90-135 | 135-180 | 0-45 | 45-90 | 90-135 | 135-180 |
| 0-10 | 0 | 0 | | | 0 | | | |
| 10-25 | 0 | 1 | | | 0 | | | |
| 25-50 | 0 | 0 | | | 0 | | | |
| 50-100 | 0 | 0 | | | 0 | | | |
| 100-250 | 0 | 0 | | | 0 | | | |
| 250-500 | 0 | 0 | | | 1 | | | |
| 500-1000 | 0 | 0 | | | | | | |
| 1000-2500 | 1 | 0 | | | | | | |
| Total | 2 | | | | | | | |

# Annex B Multiple plate targets

Experiment: 3864

Projectile: Steel

Target: Helicopter

Velocity (m/s): 2420

| Emission Angle Segment (°) | Number of Perforations per Sector | | | | | | | | | | | | | | | |
|---|---|---|---|---|---|---|---|---|---|---|---|---|---|---|---|---|
| | Plate 2 | | | | Plate 3 | | | | Plate 4 | | | | Plate 5 | | | |
| | 0-45 | 45-90 | 90-135 | 135-180 | 0-45 | 45-90 | 90-135 | 135-180 | 0-45 | 45-90 | 90-135 | 135-180 | 0-45 | 45-90 | 90-135 | 135-180 |
| 0-5 | | | | 0 | | | | | | | | | | | | |
| 5-10 | | | | 0 | | | | | | | | | | | | |
| 10-15 | | | | 0 | | | | | | | | | | | | |
| 15-20 | | | | 0 | | | | | | | | | | | | |
| 20-25 | | | | 0 | | | | | | | | | | | | |
| 25-30 | | | | 3 | | | | | | | | | | | | |
| 30-35 | | | | 3 | | | | | | | | | | | | |
| 35-40 | | | | 0 | | | | | | | | | | | | |
| 40-45 | | | | | | | | | | | | | | | | |
| 45-50 | | | | | | | | | | | | | | | | |

| Area Class ($mm^2$) | Number of Holes per Area Class in Sector | | | | | | | | | | | | | | | |
|---|---|---|---|---|---|---|---|---|---|---|---|---|---|---|---|---|
| | Plate 2 | | | | Plate 3 | | | | Plate 4 | | | | Plate 5 | | | |
| | 0-45 | 45-90 | 90-135 | 135-180 | 0-45 | 45-90 | 90-135 | 135-180 | 0-45 | 45-90 | 90-135 | 135-180 | 0-45 | 45-90 | 90-135 | 135-180 |
| 0-10 | | | | 1 | | | | | | | | | | | | |
| 10-25 | | | | 1 | | | | | | | | | | | | |
| 25-50 | | | | 2 | | | | | | | | | | | | |
| 50-100 | | | | 1 | | | | | | | | | | | | |
| 100-250 | | | | 1 | | | | | | | | | | | | |
| 250-500 | | | | | | | | | | | | | | | | |
| 500-1000 | | | | | | | | | | | | | | | | |
| Total | 6 | | | | 0 | | | | 0 | | | | 0 | | | |

Experiment: 3865
Projectile: Tungsten
Target: Helicopter
Velocity (m/s): 1750

Number of Perforations per Sector

| Emission Angle Segment (°) | Plate 2 | | | | Plate 3 | | | | Plate 4 | | | | Plate 5 | | | | Plate 6 | | | |
|---|---|---|---|---|---|---|---|---|---|---|---|---|---|---|---|---|---|---|---|---|
| | 0-45 | 45-90 | 90-135 | 135-180 | 0-45 | 45-90 | 90-135 | 135-180 | 0-45 | 45-90 | 90-135 | 135-180 | 0-45 | 45-90 | 90-135 | 135-180 | 0-45 | 45-90 | 90-135 | 135-180 |
| 0-5 | | | 0 | 5 | | | 0 | 5 | | | | 0 | | | | 0 | | | | 2 |
| 5-10 | | | 0 | 15 | | | 0 | 15 | | | | 10 | | | | 13 | | | | 5 |
| 10-15 | | | 0 | 6 | | | 0 | 6 | | | | 3 | | | | 1 | | | | 0 |
| 15-20 | | | 1 | 4 | | | 1 | 4 | | | | 0 | | | | 0 | | | | 0 |
| 20-25 | | | 1 | 2 | | | 1 | 2 | | | | 0 | | | | 0 | | | | 0 |
| 25-30 | | | 0 | 3 | | | 0 | 3 | | | | 0 | | | | 0 | | | | 0 |
| 30-35 | | | 0 | 4 | | | 0 | 4 | | | | 0 | | | | 0 | | | | 0 |
| 35-40 | | | 0 | 1 | | | 0 | 1 | | | | 0 | | | | 0 | | | | 0 |
| 40-45 | | | | | | | | | | | | | | | | | | | | |
| 45-50 | | | | | | | | | | | | | | | | | | | | |

Number of Holes per Area Class in Sector

| Area Class ($mm^2$) | Plate 2 | | | | Plate 3 | | | | Plate 4 | | | | Plate 5 | | | | Plate 6 | | | |
|---|---|---|---|---|---|---|---|---|---|---|---|---|---|---|---|---|---|---|---|---|
| | 0-45 | 45-90 | 90-135 | 135-180 | 0-45 | 45-90 | 90-135 | 135-180 | 0-45 | 45-90 | 90-135 | 135-180 | 0-45 | 45-90 | 90-135 | 135-180 | 0-45 | 45-90 | 90-135 | 135-180 |
| 0-10 | | | 0 | 15 | | | 0 | 15 | | | | 4 | | | | 7 | | | | 2 |
| 10-25 | | | 0 | 11 | | | 0 | 11 | | | | 7 | | | | 4 | | | | 1 |
| 25-50 | | | 1 | 5 | | | 1 | 5 | | | | 2 | | | | 3 | | | | 4 |
| 50-100 | | | 1 | 6 | | | 1 | 6 | | | | | | | | | | | | |
| 100-250 | | | 0 | 3 | | | 0 | 3 | | | | | | | | | | | | |
| 250-500 | | | | | | | | | | | | | | | | | | | | |
| 500-1000 | | | | | | | | | | | | | | | | | | | | |
| Total | | | 42 | | | | 42 | | | | 13 | | | | 14 | | | | 7 | |

Experiment: 3867
Projectile: Tungsten
Target: Helicopter
Velocity (m/s): 2084

Number of Perforations per Sector

| Emission Angle Segment (°) | Plate 2 | | | | Plate 3 | | | | Plate 4 | | | | Plate 5 | | | | Plate 6 | | | |
|---|---|---|---|---|---|---|---|---|---|---|---|---|---|---|---|---|---|---|---|---|
| | 0-45 | 45-90 | 90-135 | 135-180 | 0-45 | 45-90 | 90-135 | 135-180 | 0-45 | 45-90 | 90-135 | 135-180 | 0-45 | 45-90 | 90-135 | 135-180 | 0-45 | 45-90 | 90-135 | 135-180 |
| 0-5 | | | 1 | 4 | | | 0 | 8 | | | 1 | 5 | | | | 8 | | | | 2 |
| 5-10 | | | 2 | 13 | | | 5 | 54 | | | 3 | 46 | | | | 26 | | | | 15 |
| 10-15 | | | 1 | 22 | | | 0 | 16 | | | 0 | 11 | | | | 1 | | | | 0 |
| 15-20 | | | 1 | 18 | | | 0 | 5 | | | 0 | 1 | | | | 0 | | | | 0 |
| 20-25 | | | 0 | 12 | | | 0 | 3 | | | 0 | 0 | | | | 0 | | | | 0 |
| 25-30 | | | 0 | 10 | | | 0 | 0 | | | 0 | 0 | | | | 0 | | | | 0 |
| 30-35 | | | 0 | 11 | | | 0 | 0 | | | 0 | 0 | | | | 0 | | | | 0 |
| 35-40 | | | 0 | 1 | | | 0 | 0 | | | 0 | 0 | | | | 0 | | | | 0 |
| 40-45 | | | | | | | | | | | | | | | | | | | | |
| 45-50 | | | | | | | | | | | | | | | | | | | | |

Number of Holes per Area Class in Sector

| Area Class ($mm^2$) | Plate 2 | | | | Plate 3 | | | | Plate 4 | | | | Plate 5 | | | | Plate 6 | | | |
|---|---|---|---|---|---|---|---|---|---|---|---|---|---|---|---|---|---|---|---|---|
| | 0-45 | 45-90 | 90-135 | 135-180 | 0-45 | 45-90 | 90-135 | 135-180 | 0-45 | 45-90 | 90-135 | 135-180 | 0-45 | 45-90 | 90-135 | 135-180 | 0-45 | 45-90 | 90-135 | 135-180 |
| 0-10 | | | 2 | 52 | | | 5 | 71 | | | 3 | 50 | | | | 25 | | | | 12 |
| 10-25 | | | 2 | 14 | | | 0 | 6 | | | 1 | 11 | | | | 8 | | | | 5 |
| 25-50 | | | 0 | 15 | | | 0 | 6 | | | 0 | 2 | | | | 2 | | | | |
| 50-100 | | | 1 | 7 | | | 0 | 3 | | | | | | | | | | | | |
| 100-250 | | | 0 | 2 | | | | | | | | | | | | | | | | |
| 250-500 | | | 0 | 1 | | | | | | | | | | | | | | | | |
| 500-1000 | | | | | | | | | | | | | | | | | | | | |
| Total | | | 96 | | | | 91 | | | | 67 | | | | 35 | | | | 17 | |

Experiment: 3886
Projectile: Tungsten
Target: Helicopter
Velocity (m/s): 2486

Number of Perforations per Sector

| Emission Angle Segment (°) | Plate 2 | | | | Plate 3 | | | | Plate 4 | | | | Plate 5 | | | | Plate 6 | | | |
|---|---|---|---|---|---|---|---|---|---|---|---|---|---|---|---|---|---|---|---|---|
| | 0-45 | 45-90 | 90-135 | 135-180 | 0-45 | 45-90 | 90-135 | 135-180 | 0-45 | 45-90 | 90-135 | 135-180 | 0-45 | 45-90 | 90-135 | 135-180 | 0-45 | 45-90 | 90-135 | 135-180 |
| 0-5 | | | 0 | 3 | | 1 | 4 | 11 | | 1 | 1 | 3 | | | 0 | 3 | | | | 1 |
| 5-10 | | | 11 | 14 | | 0 | 12 | 58 | | 0 | 12 | 38 | | | 6 | 24 | | | | 11 |
| 10-15 | | | 5 | 22 | | 0 | 7 | 13 | | 0 | 4 | 11 | | | 1 | 3 | | | | 0 |
| 15-20 | | | 0 | 14 | | 1 | 1 | 5 | | 0 | 0 | 0 | | | 0 | 0 | | | | 0 |
| 20-25 | | | 2 | 12 | | 0 | 0 | 4 | | 0 | 0 | 0 | | | 0 | 0 | | | | 0 |
| 25-30 | | | 1 | 16 | | 0 | 0 | 0 | | 0 | 0 | 0 | | | 0 | 0 | | | | 0 |
| 30-35 | | | 0 | 6 | | 0 | 0 | 0 | | 0 | 0 | 0 | | | 0 | 0 | | | | 0 |
| 35-40 | | | 0 | 4 | | 0 | 0 | 0 | | 0 | 0 | 0 | | | 0 | 0 | | | | 0 |
| 40-45 | | | | | | | | | | | | | | | | | | | | |
| 45-50 | | | | | | | | | | | | | | | | | | | | |

Number of Holes per Area Class in Sector

| Area Class ($mm^2$) | Plate 2 | | | | Plate 3 | | | | Plate 4 | | | | Plate 5 | | | | Plate 6 | | | |
|---|---|---|---|---|---|---|---|---|---|---|---|---|---|---|---|---|---|---|---|---|
| | 0-45 | 45-90 | 90-135 | 135-180 | 0-45 | 45-90 | 90-135 | 135-180 | 0-45 | 45-90 | 90-135 | 135-180 | 0-45 | 45-90 | 90-135 | 135-180 | 0-45 | 45-90 | 90-135 | 135-180 |
| 0-10 | | | 11 | 48 | | 2 | 20 | 77 | | 1 | 15 | 46 | | | 7 | 26 | | | | 9 |
| 10-25 | | | 4 | 16 | | 0 | 4 | 10 | | 0 | 2 | 6 | | | 0 | 4 | | | | 3 |
| 25-50 | | | 3 | 15 | | 0 | 0 | 4 | | | | | | | | | | | | |
| 50-100 | | | 1 | 8 | | | | | | | | | | | | | | | | |
| 100-250 | | | 0 | 3 | | | | | | | | | | | | | | | | |
| 250-500 | | | 0 | 1 | | | | | | | | | | | | | | | | |
| 500-1000 | | | | | | | | | | | | | | | | | | | | |
| Total | | | 110 | | | | 117 | | | | 70 | | | | 37 | | | | 12 | |

# REPORT DOCUMENTATION PAGE
## (MOD-NL)

| 1. DEFENCE REPORT NO. (MOD-NL) | 2. RECIPIENT'S ACCESSION NO. | 3. PERFORMING ORGANIZATION REPORT NO. |
|---|---|---|
| TD97-0292 | | PML 1997-A65 |
| **4. PROJECT/TASK/WORK UNIT NO.** | **5. CONTRACT NO.** | **6. REPORT DATE** |
| 231494329 | A94KLu423 | December 1997 |
| **7. NUMBER OF PAGES** | **8. NUMBER OF REFERENCES** | **9. TYPE OF REPORT AND DATES COVERED** |
| 42 (incl. 1 annex, excl. RDP & distribution list) | 6 | Final |

**10. TITLE AND SUBTITLE**

Behind-armour Debris Modelling for High-velocity Fragment Impact (Part 2)

**11. AUTHOR(S)**

Dr. J.L. Verolme

**12. PERFORMING ORGANIZATION NAME(S) AND ADDRESS(ES)**

TNO Prins Maurits Laboratory, P.O. Box 45, 2280 AA Rijswijk, The Netherlands
Lange Kleiweg 137, Rijswijk, The Netherlands

**13. SPONSORING AGENCY NAME(S) AND ADDRESS(ES)**

DMKLu/WO, P.O. Box 20703, 2500 ES The Hague, The Netherlands

**14. SUPPLEMENTARY NOTES**

The classification designation Ongerubriceerd is equivalent to Unclassified.

**15. ABSTRACT (MAXIMUM 200 WORDS (1044 BYTE))**

This report presents the results of impact experiments and a parallel simulation/modelling thereof, with the main objective to study the fragmentation properties of tungsten and steel projectiles at impact. For this purpose, right circular cylinders were fired at armour steel plates. In these experiments the characterisation of the behind-armour debris (fragmentation properties) was performed by means of metallic witness packs. In addition, the interaction of the same cylinders with an array of plates representing an armoured helicopter was studied. The latter case represents an impact event, and allows a validation of the fragmentation model to be developed.
The fragmentation model uses a combination of hydrocode simulation results and semi-empirical relations to predict the characteristics of the cloud of debris formed behind the armour by the interaction of projectile and armour. The model is sofar only capable of handling normal impact.
Considering the inherent stochastic nature of fragmentation, the results are very encouraging. A first estimate of the number of perforations in the first witness pack plate can be generated.
Modeling work in the future should enhance the modelling capability, by studying the oblique impact results and the damage to the multiple-plate targets. Also, to broaden the experimental database, modern structural materials often used in flying weapon platforms will be considered.

**16. DESCRIPTORS**

Behind armor effects
High velocity
Fragmentation
Armor plate
Impact tests
Projectiles
Steel
Tungsten
Models

| 17a. SECURITY CLASSIFICATION (OF REPORT) | 17b. SECURITY CLASSIFICATION (OF PAGE) | 17c. SECURITY CLASSIFICATION (OF ABSTRACT) |
|---|---|---|
| Ongerubriceerd | Ongerubriceerd | Ongerubriceerd |

**18. DISTRIBUTION AVAILABILITY STATEMENT**

Unlimited Distribution

**17d. SECURITY CLASSIFICATION (OF TITLES)**

Ongerubriceerd

Distributielijst*

| | |
|---|---|
| 1*/2* | DWOO |
| 3 | DWOO |
| 4* | HWO-KL |
| 5 | HWO-KLu |
| 6* | HWO-KM |
| 7* | HWO-CO |
| 8 | DMKLu/WO<br>Maj. ir. J.H.J. Verhulst |
| 9 | DMKL/MUN<br>Ing. J.C. Hoeneveld |
| 10 | Bureau TNO-DO |
| 11* | Bureau TNO-DO, accountcoördinator KLu |
| 12/14 | Bibliotheek KMA |
| 15* | Lid Instituuts Advies Raad PML<br>Prof. B. Scarlett, M.Sc. |
| 16* | Lid Instituuts Advies Raad PML<br>Prof. ir. K.F. Wakker |
| 17* | Lid Instituuts Advies Raad PML<br>BGen. Prof. J.M.J. Bosch |
| 18* | Lid Instituuts Advies Raad PML<br>Ir. A.H.P.M. Schaeken |
| 19 | TNO-PML, Directie; daarna reserve |
| 20 | TNO-PML, Hoofd Divisie Wapens en Wapenplatformen<br>Dr. D.W. Hoffmans |
| 21/24 | TNO-PML, Divisie Wapens en Wapenplatformen, Groep Munitie-uitwerking en Ballistische bescherming<br>Dr. H.J. Reitsma, Ir. J.L.M.J. van Bree, Ing. M. Lans en Dr. ir. J.L. Verolme |
| 25/26* | TNO-PML, Divisie Wapens en Wapenplatformen, Hoofd Groep Wapeneffectiviteit<br>Ir. Z.C. Verheij |
| 27/29 | TNO-PML, Divisie Wapens en Wapenplatformen, Groep Wapeneffectiviteit<br>Dr. ir. M.P.I. Manders, Ir. P.W. Doup en Ir. E. van Meerten |
| 30 | TNO-PML, Documentatie |
| 31 | TNO-PML, Archief |

* De met een asterisk (*) gemerkte instanties/personen ontvangen uitsluitend de titelpagina, het managementuittreksel, de documentatiepagina en de distributielijst van het rapport.